Quantum atom–light interfaces in the Gaussian description for spin-1 systems

Quantum atom–light interfaces in the Gaussian description for spin-1 systems

Giorgio Colangelo[1,4,5]**, Robert J Sewell**[1,4]**, Naeimeh Behbood**[1]**,
Ferran Martin Ciurana**[1]**, Gil Triginer**[1,2] **and Morgan W Mitchell**[1,3]

[1] ICFO—Institut de Ciencies Fotoniques, Mediterranean Technology Park,
E-08860 Castelldefels, Barcelona, Spain
[2] Universitat Politecnica de Catalunya, E-08034 Barcelona, Spain
[3] ICREA—Institució Catalana de Recerca i Estudis Avançats, E-08015
Barcelona, Spain
E-mail: giorgio.colangelo@icfo.es

Abstract. We extend the covariance matrix description of atom–light quantum interfaces, originally developed for real and effective spin-1/2 atoms, to include 'spin alignment' degrees of freedom. This allows accurate modelling of optically probed spin-1 ensembles in arbitrary magnetic fields. We also include technical noise terms that are very common in experimental situations. These include magnetic field noise, variable atom number and the effect of magnetic field inhomogeneities. We demonstrate the validity of our extended model by comparing numerical simulations to a free–induction decay measurement of polarized ^{87}Rb atoms in the $f = 1$ ground state. We qualitatively and quantitatively reproduce experimental results with no free parameters. The model can be easily extended to larger spin systems, and adapted to more complicated experimental situations.

[4] These authors contributed equally to this work.

[5] Author to whom any correspondence should be addressed.

IOP Institute of Physics ⦿ DEUTSCHE PHYSIKALISCHE GESELLSCHAFT

Contents

1. Introduction

Atomic ensembles play an essential and growing role in quantum optics [1], with applications in quantum networking [2], generation of optical quantum resources [3, 4] and quantum-enhanced instruments [5–8]. The continuous-variable (CV) approach [9] efficiently describes experiments involving many quanta. The great majority of CV atomic ensemble experiments are performed with Gaussian states, although non-Gaussian atomic states [10] are required for some tasks [11]. Gaussian states can be described very economically in terms of mean values and variances, whereas general states require a description exponential in the size of the system. The Gaussian approximation can be justified via the Holstein–Primakoff approximation, including extensions to larger-spin systems [12]. We follow the approach of Kraus *et al* [13], Madsen and Mølmer [14], Hammerer *et al* [15] and Mølmer and Madsen [16] and use covariance matrix techniques to describe the collective atom and light variables and their interaction.

    A wide variety of effects, including spatial and temporal inhomogeneities, loss, decoherence, atomic transport and projective measurements have been incorporated into this framework [17]. An important omission until now has been the description of larger-spin

IOP Institute of Physics ‖ DEUTSCHE PHYSIKALISCHE GESELLSCHAFT

systems. Most atomic ensemble experiments are performed with alkali atoms and thus have ground-state spin of at least 1, which implies tensorial light shifts [14] and generalized Faraday rotation effects [18]. An extension of the covariance matrix techniques to include these effects will allow statistical description of many large-spin applications [19], including quantum state characterization [20] and preparation [21], quantum chaos [22], optical magnetometry [8, 23, 24] and quantum non-demolition measurement [25, 26].

While several earlier works have applied the spin-1/2 framework to spin-1 or larger systems through the identification of a two-state 'pseudo spin-1/2' sub-system, there are scenarios in which the dynamics naturally involves more than two levels, and requires a more expanded description. A clear example is a spin-1 or larger atom in the presence of both magnetic and optical fields. The magnetic field couples Zeeman states differing by $\Delta m = \pm 1$, whereas the optical fields couple also states with $\Delta m = \pm 2$ through tensorial light shifts. This system has been much studied using density-matrix approaches [20], which describe fully the average single-atom properties but not the noise properties, which arise from correlations among the atoms. Consideration of the quantum noise in these systems motivates the current work, in which we extend the covariance matrix approach to spin-1 atoms. To the suite of techniques available for spin-1/2 ensembles [14, 17], we add the ability to treat both vectorial and tensorial light shifts, technical noise due to uncertainty in the atom number and dephasing due to magnetic field inhomogeneities.

The paper is organized as follows. In section 2 we present the formalism, which employs eight orientation and alignment operators to describe the $F = 1$ collective atomic spin. In section 3 we analyse the spin dynamics in the presence of probing light and an external magnetic field, including coherent evolution, decoherence due to scattering of probe photons and dephasing due to inhomogeneous magnetic fields. In section 4 we review the description of optical measurement within the covariance matrix formalism. In section 5 we describe the initial state including technical noise from uncertain atom number. In sections 6 and 7 we compare numerical results of our model with experimental data and identify the practical limits of the Gaussian approximation in this system.

2. Formalism

We work with collective operators describing macroscopic numbers of particles, for which a CV description is appropriate. Throughout, we use the covariance matrix techniques [14, 17], which are sufficient to describe the Gaussian states encountered in the great majority of CV experiments.

2.1. Quantum polarization description

Polarized light in CVs can be described with Stokes operators:

$$\hat{S}_x \equiv \tfrac{1}{2}\hat{\mathbf{a}}^\dagger \boldsymbol{\sigma}_x \hat{\mathbf{a}}, \quad \hat{S}_y \equiv \tfrac{1}{2}\hat{\mathbf{a}}^\dagger \boldsymbol{\sigma}_y \hat{\mathbf{a}}, \quad \hat{S}_z \equiv \tfrac{1}{2}\hat{\mathbf{a}}^\dagger \boldsymbol{\sigma}_z \hat{\mathbf{a}}, \quad \hat{S}_0 \equiv \tfrac{1}{2}\hat{\mathbf{a}}^\dagger \mathbb{1}\hat{\mathbf{a}}, \tag{1}$$

where $\hat{\mathbf{a}} \equiv (\hat{a}_+, \hat{a}_-)^T$ and $\hat{a}_+$, $\hat{a}_-$ are the annihilation operators for the left and right circular polarization and $\boldsymbol{\sigma}_x$, $\boldsymbol{\sigma}_y$, $\boldsymbol{\sigma}_z$ the Pauli matrices and $\mathbb{1}$ is the identity matrix. The $\hat{S}_x$, $\hat{S}_y$, $\hat{S}_z$ and $\hat{S}_0$ Stokes operators represent, respectively, linearly polarized light horizontally or vertically, linearly polarized light on the $\pm 45°$ direction, left and right circularly polarized light and the pulse energy. They have the same commutation relations as angular momentum operators, $[\hat{S}_x, \hat{S}_y] = i\hat{S}_z$ and cyclic permutations and they all commute with $\hat{S}_0$.

2.2. Description of spin-1 ensembles

A single spin-1 atom is described by a density matrix with eight degrees of freedom, which we express in terms of eight single-particle operators $\hat{\lambda}_i$. These generalize the Pauli matrices, in the sense that they are traceless, Hermitian, and obey the orthonormality relation $\text{Tr}(\lambda_i \lambda_j) = 2\delta_{ij}$. The first three operators are the components of the spin vector $\hat{\mathbf{f}}$, obeying $[\hat{f}_x, \hat{f}_y] = i\hat{f}_z$. For illustration, we give the spin-1 matrix representation:

$$\hat{f}_x \xrightarrow{F=1} \frac{1}{\sqrt{2}} \begin{pmatrix} 0 & 1 & 0 \\ 1 & 0 & 1 \\ 0 & 1 & 0 \end{pmatrix},$$

$$\hat{f}_y \xrightarrow{F=1} \frac{1}{\sqrt{2}} \begin{pmatrix} 0 & -i & 0 \\ i & 0 & -i \\ 0 & i & 0 \end{pmatrix},$$

$$\hat{f}_z \xrightarrow{F=1} \begin{pmatrix} 1 & 0 & 0 \\ 0 & 0 & 0 \\ 0 & 0 & -1 \end{pmatrix}.$$

The others are rank-2 tensor operators, for which we use the symbol $\hat{\mathbf{j}}$, with components (again with the spin-1 representation for illustration):

$$\hat{j}_x \equiv \hat{f}_x^2 - \hat{f}_y^2 \xrightarrow{F=1} \begin{pmatrix} 0 & 0 & 1 \\ 0 & 0 & 0 \\ 1 & 0 & 0 \end{pmatrix},$$

$$\hat{j}_y \equiv \hat{f}_x \hat{f}_y + \hat{f}_y \hat{f}_x \xrightarrow{F=1} \begin{pmatrix} 0 & 0 & -i \\ 0 & 0 & 0 \\ i & 0 & 0 \end{pmatrix},$$

$$\hat{j}_k \equiv \hat{f}_x \hat{f}_z + \hat{f}_z \hat{f}_x \xrightarrow{F=1} \frac{1}{\sqrt{2}} \begin{pmatrix} 0 & 1 & 0 \\ 1 & 0 & -1 \\ 0 & -1 & 0 \end{pmatrix},$$

$$\hat{j}_l \equiv \hat{f}_y \hat{f}_z + \hat{f}_z \hat{f}_y \xrightarrow{F=1} \frac{1}{\sqrt{2}} \begin{pmatrix} 0 & -i & 0 \\ i & 0 & i \\ 0 & -i & 0 \end{pmatrix},$$

$$\hat{j}_m \equiv \frac{1}{\sqrt{3}} (2\hat{f}_z^2 - \hat{f}_x^2 - \hat{f}_y^2) \xrightarrow{F=1} \frac{1}{\sqrt{3}} \begin{pmatrix} 1 & 0 & 0 \\ 0 & -2 & 0 \\ 0 & 0 & 1 \end{pmatrix}.$$
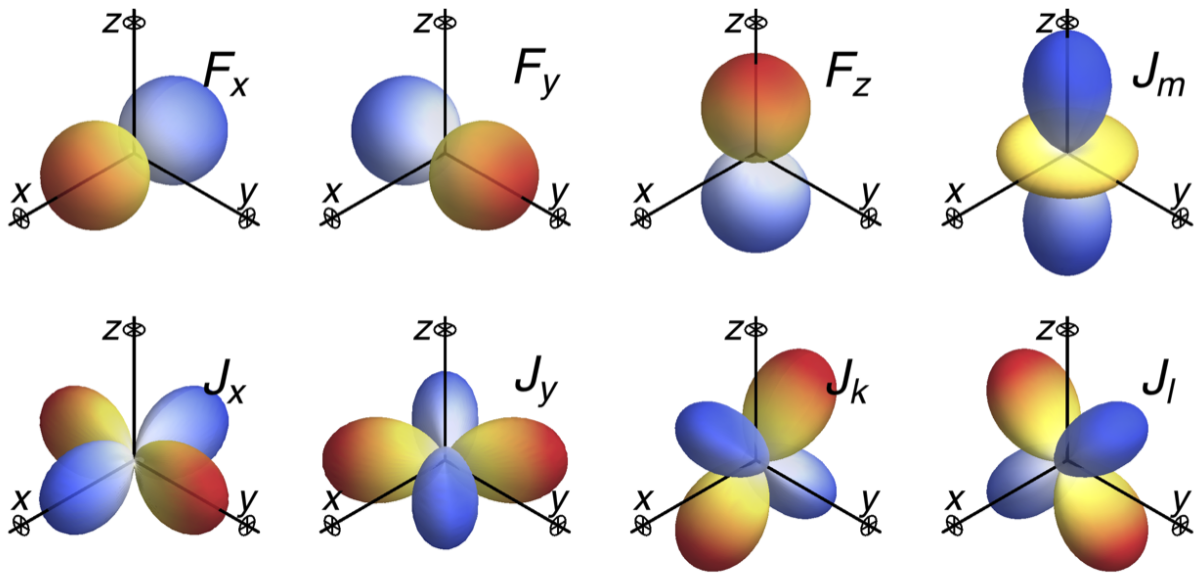
Figure 1. Contribution $dW/d\bar{\lambda}_i$ of the f and j operators to the Wigner distribution $W_\rho(\theta, \phi)$ representing the state $\rho = \frac{1}{3}\mathbf{I} + \frac{1}{2}\sum_i \hat{\lambda}_i \bar{\lambda}_i$, as described in [28]. Radius indicates magnitude, warm (cold) colours indicate positive (negative) contributions. Axis markers indicate unity.

With quantization axis along z, $\hat{j}_m$ describes the population imbalance between $m_F = 0$ and other states, while $\hat{j}_{x,y}$ describe $m_F = \pm 1$ coherences. $\hat{j}_{k,l}$ represent $m_F = \pm 1$ coherences in other quantization axes.

We note that the above operator definitions are spin-independent, and that the results in this paper follow from these operator definitions, not from the spin-1-specific matrix representations. As we shall see below, the most important coherent interactions: Larmor precession, Faraday rotation and tensorial light shifts, can be fully described using the above operators, even for larger spin. The formalism developed here is thus applicable to some scenarios involving spin-3/2 and higher. Not all processes can be explained using just $\hat{\mathbf{f}}$ and $\hat{\mathbf{j}}$ operators, however. For example, with spin-2 atoms modulated optical pumping in the presence of a B-field has been used to produce hexadecapole moment due to coherence between Zeeman states with $\Delta m_F = 4$ [27].

2.3. Spin visualization

From the orthogonality relation $\mathrm{Tr}[\lambda_i \lambda_j] = 2\delta_{ij}$, an arbitrary single-atom density matrix ρ can be expressed as

$$\rho = \frac{1}{3}\mathbf{I} + \frac{1}{2}\sum_i \hat{\lambda}_i \bar{\lambda}_j, \tag{2}$$

where $\bar{\lambda}_i \equiv \mathrm{Tr}[\rho\hat{\lambda}_i]$. This suggests a visualization in terms of the spin Wigner distribution $W(\rho)$, which is efficiently calculated as in Dowling *et al* [28]. In figure 1 we show the differential contribution to the Wigner distribution $dW/d\bar{\lambda}_i$. This shows, for example, that any of $\hat{j}_x$, $\hat{j}_y$, $\hat{j}_k$ and $\hat{j}_l$ can be obtained by rotation of $\hat{j}_x$, whereas $\hat{j}_m$ cannot.

Table 1. Commutation relationships for single-atom operators.

$[\,,\,]$	$\hat{f}_x$	$\hat{f}_y$	$\hat{f}_z$	$\hat{j}_x$	$\hat{j}_y$	$\hat{j}_k$	$\hat{j}_l$	$\hat{j}_m$
$\hat{f}_x$	0	$\hat{f}_z$	$-\hat{f}_y$	$-\hat{j}_l$	$\hat{j}_k$	$-\hat{j}_y$	$\sqrt{3}\hat{j}_m+\hat{j}_x$	$-\sqrt{3}\hat{j}_l$
$\hat{f}_y$	$-\hat{f}_z$	0	$\hat{f}_x$	$-\hat{j}_k$	$-\hat{j}_l$	$-\sqrt{3}\hat{j}_m+\hat{j}_x$	$\hat{j}_y$	$\sqrt{3}\hat{j}_k$
$\hat{f}_z$	$\hat{f}_y$	$-\hat{f}_x$	0	$2\hat{j}_y$	$-2\hat{j}_x$	$\hat{j}_l$	$-\hat{j}_k$	0
$\hat{j}_x$	$\hat{j}_l$	$\hat{j}_k$	$-2\hat{j}_y$	0	$2\hat{f}_z$	$-\hat{f}_y$	$\hat{f}_x$	0
$\hat{j}_y$	$-\hat{j}_k$	$\hat{j}_l$	$2\hat{j}_x$	$-2\hat{f}_z$	0	$\hat{f}_x$	$-\hat{f}_y$	0
$\hat{j}_k$	$\hat{j}_y$	$\sqrt{3}\hat{j}_m-\hat{j}_x$	$-\hat{j}_l$	$\hat{f}_y$	$-\hat{f}_x$	0	$\hat{f}_z$	$-\sqrt{3}\hat{f}_y$
$\hat{j}_l$	$-\sqrt{3}\hat{j}_m-\hat{j}_x$	$-\hat{j}_y$	$\hat{j}_k$	$\hat{f}_x$	$\hat{f}_y$	$-\hat{f}_z$	0	$\sqrt{3}\hat{f}_x$
$\hat{j}_m$	$\sqrt{3}\hat{j}_l$	$-\sqrt{3}\hat{j}_k$	0	0	0	$\sqrt{3}\hat{f}_y$	$-\sqrt{3}\hat{f}_x$	0

2.4. Commutation relationships

The operators $\hat{\mathbf{f}}$, $\hat{\mathbf{j}}$ and $\hat{\mathbf{S}}$ have commutators given by

$$[\hat{\lambda}_a, \hat{\lambda}_b] = \mathrm{i}c^{\hat{\lambda}_a\hat{\lambda}_b}_{\hat{\lambda}_k}\hat{\lambda}_k, \tag{3}$$

where the $\hat{\lambda}$ are $\hat{\mathbf{f}}$ or $\hat{\mathbf{j}}$ components and a sum is over k is implied. The structure constants $c^{\hat{\lambda}_a\hat{\lambda}_b}_{\hat{\lambda}_k}$ are completely antisymmetric in the three indexes, and

$$c^{\hat{f}_x\hat{f}_y}_{\hat{f}_z} = 1, \quad c^{\hat{j}_x\hat{j}_y}_{\hat{f}_z} = 2, \quad c^{\hat{f}_x\hat{j}_l}_{\hat{j}_m} = c^{\hat{f}_y\hat{j}_m}_{\hat{j}_k} = \sqrt{3}, \tag{4}$$

$$c^{\hat{f}_x\hat{j}_y}_{\hat{j}_k} = c^{\hat{f}_x\hat{j}_l}_{\hat{j}_x} = c^{\hat{f}_y\hat{j}_k}_{\hat{j}_x} = c^{\hat{f}_z\hat{j}_k}_{\hat{j}_l} = 1. \tag{5}$$

To this we can add

$$c^{\hat{S}_x\hat{S}_y}_{\hat{S}_z} = 1. \tag{6}$$

All structure constants not given above are zero. The commutators are given explicitly in table 1.

2.5. Collective spin operators

To describe the ensemble we define collective operators. If $\hat{\boldsymbol{\lambda}}^{(i)}$ describes atomic operators acting the ith of N_A atoms, then $\hat{\boldsymbol{\Lambda}} \equiv \sum_i^{N_A} \hat{\boldsymbol{\lambda}}^{(i)}$. Explicitly for the vector ($\hat{\mathbf{f}}$) and tensor ($\hat{\mathbf{j}}$) collective spin operators:

$$\hat{\mathbf{F}} \equiv \sum_{i=1}^{N_A} \hat{\mathbf{f}}^{(i)}, \quad \hat{\mathbf{J}} \equiv \sum_{i=1}^{N_A} \hat{\mathbf{j}}^{(i)}. \tag{7}$$

We note that these inherit their commutation relations from the microscopic operators: $[\hat{\Lambda}_a, \hat{\Lambda}_b] = \mathrm{i}c^{\hat{\lambda}_a\hat{\lambda}_b}_{\hat{\lambda}_k}\hat{\Lambda}_k$. Finally, we define a phase-space vector to describe the state of the whole system

$$\hat{\mathbf{V}} = \mathbf{B} \oplus \hat{\mathbf{F}} \oplus \hat{\mathbf{J}} \oplus \bigoplus_{i=1}^{N_{\text{pulses}}} \hat{\mathbf{S}}^{(i)}, \tag{8}$$

IOP Institute of Physics Φ DEUTSCHE PHYSIKALISCHE GESELLSCHAFT

where $\oplus$ indicates the direct sum and $\mathbf{B}$ is the magnetic field vector at the location of the ensemble. It should be noted that $\mathbf{B}$ is here a classical field, whereas the other components of $\hat{\mathbf{V}}$ are operators. The inclusion of $\mathbf{B}$ in $\hat{\mathbf{V}}$ allows for classical uncertainty about the field to be incorporated in a natural way into the calculations [14], as we describe below.

2.6. Covariance matrix

We work within the Gaussian approximation, i.e. we assume that $\hat{\mathbf{V}}$ is fully characterized by its average $\langle \hat{\mathbf{V}} \rangle$ and by its covariance matrix $\Gamma_{\mathbf{V}}$:

$$\Gamma_{\mathbf{V}} \equiv \tfrac{1}{2} \langle \hat{\mathbf{V}} \wedge \hat{\mathbf{V}} + (\hat{\mathbf{V}} \wedge \hat{\mathbf{V}})^{\mathrm{T}} \rangle - \langle \hat{\mathbf{V}} \rangle \wedge \langle \hat{\mathbf{V}} \rangle, \tag{9}$$

where $\wedge$ indicates the outer product. It will be convenient to define $\delta\hat{\mathbf{V}} \equiv \hat{\mathbf{V}} - \langle \hat{\mathbf{V}} \rangle$, the fluctuations of $\hat{\mathbf{V}}$ about the mean, from which $\Gamma_{\mathbf{V}} = \tfrac{1}{2} \langle \delta\hat{\mathbf{V}} \wedge \delta\hat{\mathbf{V}} + (\delta\hat{\mathbf{V}} \wedge \delta\hat{\mathbf{V}})^{\mathrm{T}} \rangle$.

3. Dynamics

We describe the most important dynamical effects for light–matter interfaces, namely the light–matter interaction that occurs when a pulse of probe light passes the ensemble, and the rotation due to a magnetic field. Both of these interactions produce coherent rotations, loss of coherence and addition of noise.

3.1. Light–atom interactions

The light–atom interaction is described by an effective Hamiltonian which describes the dispersive effects of the electric dipole interaction in second order [29–31]. In simulations and in practice, it is very convenient to employ a train of optical pulses for probing the ensemble. Even for continuous probing it is useful to treat the probe as a train of continuous pulses, as this allows a course-grained description of the polarization evolution [14, 16]. In $F = 1$ atomic ensembles, during the time the mth pulse is passing through the ensemble, the effective Hamiltonian is

$$H_{\mathrm{eff}}^{(m)} = G_1 \frac{\hat{S}_z^{(m)}}{\tau} \hat{F}_z + G_2 \left(\frac{\hat{S}_x^{(m)}}{\tau} \hat{J}_x + \frac{\hat{S}_y^{(m)}}{\tau} \hat{J}_y + \frac{1}{\sqrt{3}} \frac{\hat{S}_0^{(m)}}{\tau} \hat{J}_m \right), \tag{10}$$

where G_1 and G_2 are coupling constants that depend on the geometry of the atomic ensemble and probe beam, the atomic structure and the detuning from resonance [30]. In situations where the approximation of homogeneous interaction breaks down, it is possible to model the system as in [17] by breaking it into smaller subsystems each of which is effectively homogeneous. In the situations simulated in sections 6 and 7, the inhomogeneous coupling is due to the spatial distribution of atoms within a Gaussian probe beam, and is estimated to be a small effect for the examples discussed in this paper. We label the Stokes operators as $\hat{\mathbf{S}}^{(m)}(t)$, $m = 1, \ldots, N_{\mathrm{pulses}}$ where t_m indicates the time of arrival at the ensemble. Thus $\hat{\mathbf{S}}^{(m)}(t < t_m)$ describes the polarization of the mth pulse before entering the ensemble, while $\hat{\mathbf{S}}^{(m)}(t > t_m + \tau)$, where τ is the pulse duration, describes the polarization of the same pulse after exiting the ensemble. At time $t_m + \tau$, the mth pulse has left the ensemble (we assume the transit time is much less than τ) and the change in the system is described by

$$\hat{\mathbf{\Lambda}}(t_m + \tau) = \hat{\mathbf{\Lambda}}(t_m) - \mathrm{i}\tau [\hat{\mathbf{\Lambda}}(t_m), H_{\mathrm{eff}}^{(m)}] \tag{11}$$

and

$$\hat{\mathbf{S}}^{(m)}(t_m + \tau) = \hat{\mathbf{S}}^{(m)}(t_m) - \mathrm{i}\tau[\hat{\mathbf{S}}^{(m)}(t_m), H_{\mathrm{eff}}^{(m)}]. \tag{12}$$

All other polarizations $\hat{\mathbf{S}}^{(n)}$, $n \neq m$ are unchanged. These first-order difference equations will be accurate for sufficiently low-energy pulses, i.e. for small $G_{1,2}\langle\hat{\mathbf{S}}\rangle$. For any given physical situation these conditions can be satisfied by subdividing long- or high-energy pulses into subpulses with smaller τ, at the cost of additional computation time. Similarly, if the full ensemble produces large rotations of $\hat{\mathbf{S}}$, the $\hat{\mathbf{\Lambda}}$ can be subdivided as in Koschorreck and Mitchell [17]. In the simulations described below we subdivide $\hat{\mathbf{S}}$ until the results converge.

The evolution is compactly expressed in terms of a tensor $\mathbf{H}^{(m)}$ containing the coupling constants $G_{1,2}$ and $g_F\mu_0$ and the structure factors $c_{\hat{V}_k}^{\hat{V}_i\hat{V}_j}$:

$$\hat{V}_i(t_m + \tau) = \hat{V}_i(t_m) + \hat{V}_j(t_m) H_{jk}^{i(m)} \hat{V}_k(t_m) \quad \text{where} \tag{13}$$

$$H_{jk}^{i(m)} \equiv G_1 \delta_{\hat{V}_j}^{\hat{S}_z^{(m)}} c_{\hat{V}_k}^{\hat{V}_i\hat{j}_z} + G_2 \left(\delta_{\hat{V}_j}^{\hat{S}_x^{(m)}} c_{\hat{V}_k}^{\hat{V}_i\hat{j}_x} + \delta_{\hat{V}_j}^{\hat{S}_y^{(m)}} c_{\hat{V}_k}^{\hat{V}_i\hat{j}_y} + \frac{1}{\sqrt{3}} \delta_{\hat{V}_j}^{\hat{S}_0^{(m)}} c_{\hat{V}_k}^{\hat{V}_iJm} \right), \tag{14}$$

where $\delta_{\hat{V}_i}^{\hat{V}_j}$ is 1 for $\hat{V}_i = \hat{V}_j$ and 0 for $\hat{V}_i \neq \hat{V}_j$, and we assume summation over repeated indices.

3.2. Linearization

The difference equation (13) are bilinear in the components of $\hat{\mathbf{V}}$. Although nonlinearity can in some cases lead to non-Gaussian phase-space distributions [22, 32], in practice Gaussian or near-Gaussian distributions are far more common, and indeed producing measurably non-Gaussian distributions is non-trivial [10]. This motivates a linearization of the above equations. Symbolically we write

$$\hat{\mathbf{V}}(t_m + \tau) = \hat{\mathbf{V}}(t_m) + \hat{\mathbf{V}}(t_m) \cdot \mathbf{H}^{(m)} \cdot \hat{\mathbf{V}}(t_m) \tag{15}$$

and separate $\hat{\mathbf{V}}$ into the average $\bar{\mathbf{V}}$ and the fluctuations $\delta\hat{\mathbf{V}}$:

$$
\begin{aligned}
\hat{\mathbf{V}}(t_m + \tau) &= \bar{\mathbf{V}}(t_m + \tau) + \delta\hat{\mathbf{V}}(t_m + \tau) \\
&= \bar{\mathbf{V}}(t_m) + \bar{\mathbf{V}}(t_m) \cdot \mathbf{H}^{(m)} \cdot \bar{\mathbf{V}}(t_m) + \delta\hat{\mathbf{V}}(t_m) + \bar{\mathbf{V}}(t_m) \cdot \mathbf{H}^{(m)} \cdot \delta\hat{\mathbf{V}}(t_m) \\
&\quad + \delta\hat{\mathbf{V}}(t_m) \cdot \mathbf{H}^{(m)} \cdot \bar{\mathbf{V}}(t_m) + \delta\hat{\mathbf{V}}(t_m) \cdot \mathbf{H}^{(m)} \cdot \delta\hat{\mathbf{V}}(t_m).
\end{aligned}
\tag{16}
$$

When the last term can be neglected, the dynamics reduce to

$$\bar{\mathbf{V}}(t_m + \tau) = \bar{\mathbf{V}}(t_m) + \bar{\mathbf{V}}(t_m) \cdot \mathbf{H}^{(m)} \cdot \bar{\mathbf{V}}(t_m) \tag{17}$$

$$= \bar{\mathbf{V}}(t_m) + \mathbf{U}^{(m)} \cdot \bar{\mathbf{V}}(t_m), \tag{18}$$

where $\mathbf{U}^{(m)} \equiv \bar{\mathbf{V}}(t_m) \cdot \mathbf{H}^{(m)}$, which describes a nonlinear evolution of the average $\bar{\mathbf{V}}$, and

$$
\begin{aligned}
\delta\hat{\mathbf{V}}(t_m + \tau) &= \delta\hat{\mathbf{V}}(t_m) + \bar{\mathbf{V}}(t_m) \cdot \mathbf{H}^{(m)} \cdot \delta\hat{\mathbf{V}}(t_m) + \delta\hat{\mathbf{V}}(t_m) \cdot \mathbf{H}^{(m)} \cdot \bar{\mathbf{V}}(t_m) \\
&= \mathbf{T}^{(m)} \cdot \delta\hat{\mathbf{V}}(t_m),
\end{aligned}
\tag{19}
$$

which describes a linear evolution of the fluctuations $\delta\hat{\mathbf{V}}$ in terms of the matrix

$$T_{ik}^{(m)} \equiv \delta_i^k + \mathrm{V}_j H_{jk}^{i(m)+H_{kj}^{i(m)}} \mathrm{V}_j. \tag{20}$$

The covariance matrix Γ evolves as

$$\Gamma(t_m + \tau) = \mathbf{T}^{(m)} \cdot \Gamma(t_m) \cdot [\mathbf{T}^{(m)}]^{\mathrm{T}}. \tag{21}$$

3.3. Optically induced decoherence

The above coherent rotations are necessarily accompanied by spontaneous scattering of photons, which produces decoherence of the atomic state [17, 30]. An accurate treatment is possible [33], but requires a detailed accounting of the scattering channels. Here we describe a simple noise model, based on that of Madsen and Mølmer [14], which agrees reasonably well with more sophisticated models [33].

We treat the decoherence as removal of a fraction $1 - \mathcal{X}$ of the N_A atoms, followed by the re-addition of a fraction p of the removed atoms, with random polarizations. A common source of 'loss' of atoms from the system is optical pumping into dark states [30, 33]. In this paper we take $p = 1$, i.e. no loss, which gives an upper bound on the introduced decoherence. As demonstrated in appendix A, this alters the phase-space distribution as

$$\bar{\mathbf{\Lambda}} \to \mathcal{X}\bar{\mathbf{\Lambda}}, \tag{22}$$

$$\Gamma_{\mathbf{\Lambda}} \to \mathcal{X}^2 \Gamma_{\mathbf{\Lambda}} + \mathcal{X}(1 - \mathcal{X})N_A \Gamma_{\boldsymbol{\lambda}} + p(1 - \mathcal{X})\tfrac{2}{3}N_A \mathbb{1}_{8 \times 8}, \tag{23}$$

where $\bar{\mathbf{\Lambda}} \equiv \langle \hat{\Lambda} \rangle$, $\Gamma_{\mathbf{\Lambda}} \equiv \frac{1}{2}\langle \hat{\mathbf{\Lambda}} \wedge \hat{\mathbf{\Lambda}} + (\hat{\mathbf{\Lambda}} \wedge \hat{\mathbf{\Lambda}})^T \rangle - \langle \hat{\mathbf{\Lambda}} \rangle \wedge \langle \hat{\mathbf{\Lambda}} \rangle$ is the atomic part of the covariance matrix $\Gamma_{\mathbf{V}}$, $\Gamma_{\boldsymbol{\lambda}} \equiv \frac{1}{2}\langle \hat{\boldsymbol{\lambda}} \wedge \hat{\boldsymbol{\lambda}} + (\hat{\boldsymbol{\lambda}} \wedge \hat{\boldsymbol{\lambda}})^T \rangle - \langle \hat{\boldsymbol{\lambda}} \rangle \wedge \langle \hat{\boldsymbol{\lambda}} \rangle$ is the single-atom covariance matrix, and the expectations are taken with respect to the average single-atom state ρ. As derived in appendix A, $\Gamma_{\boldsymbol{\lambda}}$ can be found from $\bar{\mathbf{V}}$ as

$$\Gamma_{\boldsymbol{\lambda}} = \tfrac{2}{3}\mathbb{1}_{8 \times 8} - \bar{\boldsymbol{\lambda}} \wedge \bar{\boldsymbol{\lambda}} + \sum_k \bar{\lambda}_k \mathbf{M}^{(k)},$$
$$M_{ij}^{(k)} \equiv \tfrac{1}{4}\mathrm{Tr}[\hat{\lambda}_k \{\hat{\lambda}_i, \hat{\lambda}_j\}], \tag{24}$$

where $\bar{\boldsymbol{\lambda}} \equiv \langle \boldsymbol{\lambda} \rangle_\rho$ is the single-atom average and $\{\cdot, \cdot\}$ indicates the anti-commutator.

The transformation of the atomic covariance matrix due to optically induced decoherence is then

$$\Gamma_{\mathbf{\Lambda}}(t_m + \tau) = \mathcal{D}_{\mathbf{\Lambda}}^{(m)} \cdot \Gamma_{\mathbf{\Lambda}}(t_m + \tau) \cdot [\mathcal{D}_{\mathbf{\Lambda}}^{(m)}]^T + \mathcal{N}_{\mathbf{\Lambda}}^{(m)}, \tag{25}$$

where $\Gamma_{\mathbf{\Lambda}}(t_m + \tau)$ is given by equation (21) and

$$\mathcal{D}_{\mathbf{\Lambda}}^{(m)} \equiv \mathcal{X}\mathbb{1}_{8 \times 8}, \tag{26}$$

$$\mathcal{N}_{\mathbf{\Lambda}}^{(m)} \equiv \mathcal{X}(1 - \mathcal{X})N_A \Gamma_{\boldsymbol{\lambda}} + p(1 - \mathcal{X})\tfrac{2}{3}N_A \mathbb{1}_{8 \times 8}. \tag{27}$$

The fraction of atoms $1 - \mathcal{X}$ that experience incoherent scattering of probe photons during a single pulse of duration τ is given by $\mathcal{X} = \exp(-\eta_\gamma n_L)$, where η_γ is the probability for an atom to scatter a photon and n_L is the number of photons in the pulse. A similar decoherence applies to the optical polarization $\hat{S}^{(m)}$ [17], where the fraction of photons scattered is $1 - \epsilon$ and $\epsilon = \exp(-\eta_\gamma N_A)$, leading to decoherence and noise terms

$$\mathcal{D}_{\mathbf{S}}^{(m)} \equiv \epsilon\mathbb{1}_{3 \times 3}, \tag{28}$$

$$\mathcal{N}_{\mathbf{S}}^{(m)} \equiv \epsilon(1 - \epsilon)n_L \Gamma_{\mathbf{S}}, \tag{29}$$

where $\Gamma_{\mathbf{S}} = (1/4)\mathbb{1}_{3 \times 3}$ is the single photon covariance matrix. Because scattered photons are lost from the pulse, there is no photonic analogue of the last term of equation (27). In the scenarios described below the decoherence of the optical pulses is negligible, because the number of photons is much larger than the number of atoms, and we set $\epsilon = 1$.

The full covariance matrix Γ then evolves as

$$\Gamma(t_m + \tau) = \mathbf{D}^{(m)} \cdot \mathbf{T}^{(m)} \cdot \Gamma(t_m) \cdot [\mathbf{T}^{(m)}]^T \cdot [\mathbf{D}^{(m)}]^T + \mathbf{N}^{(m)}, \tag{30}$$

where $\mathbf{D}^{(m)} \equiv \mathbb{1}_{3 \times 3} \oplus \mathcal{D}_{\mathbf{\Lambda}}^{(m)} \oplus \mathcal{D}_{\mathbf{S}}^{(m)}$ and $\mathbf{N}^{(m)} \equiv \mathbb{0}_{3 \times 3} \oplus \mathcal{N}_{\mathbf{\Lambda}}^{(m)} \oplus \mathcal{N}_{\mathbf{S}}^{(m)}$.

3.4. Atom–field interaction

In contrast to the atom–light interaction, the interaction of the atoms with the magnetic field is purely linear, so that precession by large angles can be described in a single step. At the same time, inhomogeneities in the magnetic field introduce dephasing, which requires a different description than given above for scattering-induced decoherence[6].

To describe these effects, we first split the field into homogeneous and inhomogeneous parts as $\mathbf{B}(\mathbf{x}) = \mathbf{B}_0 + \tilde{\mathbf{B}}_1(\mathbf{x})$, with the assumption that $|\mathbf{B}_0| \gg |\tilde{\mathbf{B}}_1(\mathbf{x})|$ for $\mathbf{x}$ within the atomic cloud. Specifically, if $\rho_{\mathrm{at}}(\mathbf{x})$ is the atomic density, we take $\mathbf{B}_0 = \int \mathrm{d}^3 x \, \rho_{\mathrm{at}}(\mathbf{x}) \mathbf{B}(\mathbf{x})$, the average over the atoms.

Local rotation under $\mathbf{B}(\mathbf{x})$ can be described by the unitary operator

$$U(\mathbf{x}, t) = \exp[\mathrm{i}\gamma t |B(x)| \hat{f}_{\mathbf{B}}(x)], \tag{31}$$

where $\hat{f}_{\mathbf{B}}(x)$ is the component of $\hat{\mathbf{F}}$ parallel to the local field and $\gamma = \mu_{\mathrm{B}} g_F / \hbar$ is the gyromagnetic ratio, where g_F is the Landé factor and μ_{B} is the Bohr magneton. We note that $\hat{f}_{\mathbf{B}}^{n+2}(x) = \hat{f}_{\mathbf{B}}^n(x)$ for $n \geqslant 1$, (true for any $F = 1$ spin component), so that a Taylor expansion of U gives

$$U(\mathbf{x}, t) = \mathbb{1} + \hat{f}_{\mathbf{B}}(x) \sin(\gamma |B(x)| t) + \hat{f}_{\mathbf{B}}^2(x)[\cos(\gamma |B(x)| t) - 1]. \tag{32}$$

We can now see a qualitative difference between $\mathbf{B}_\parallel(\mathbf{x})$, the component of $\tilde{\mathbf{B}}_1(\mathbf{x})$ parallel to $\mathbf{B}_0$, and $\mathbf{B}_\perp(\mathbf{x})$ the perpendicular components. The effect of $\mathbf{B}_\parallel(\mathbf{x})$ is to change $|\mathbf{B}|$ and thus the precession frequency, causing a deviation from the behaviour under $\mathbf{B}_0$ that accumulates with time. In contrast, $\mathbf{B}_\perp(\mathbf{x})$ principally changes the direction of $\hat{f}_{\mathbf{B}}$, a non-accumulating effect. For this reason we focus on the effects of $\mathbf{B}_\parallel(\mathbf{x})$. We consider the evolution of operators $\hat{\boldsymbol{\lambda}}(\mathbf{x})$ that describe a single atom at a position $\mathbf{x}$. Using the Heisenberg equations of motion and the commutation relations of equation (3), we find dynamical equations

$$\frac{\mathrm{d}}{\mathrm{d}t} \hat{\boldsymbol{\lambda}}(\mathbf{x}) = -\mu_{\mathrm{B}} g_F |\mathbf{B}(\mathbf{x})| \mathcal{A}(\mathbf{x}) \cdot \hat{\boldsymbol{\lambda}}(\mathbf{x}), \tag{33}$$

where

$$\mathcal{A} \equiv \begin{pmatrix} \cdot & -b_z & b_y & \cdot & \cdot & \cdot & \cdot & \cdot \\ b_z & \cdot & -b_x & \cdot & \cdot & \cdot & \cdot & \cdot \\ -b_y & b_x & \cdot & \cdot & \cdot & \cdot & \cdot & \cdot \\ \cdot & \cdot & \cdot & \cdot & -2b_z & b_y & b_x & \cdot \\ \cdot & \cdot & \cdot & 2b_z & \cdot & -b_x & b_y & \cdot \\ \cdot & \cdot & \cdot & -b_y & b_x & \cdot & -b_z & \sqrt{3}b_y \\ \cdot & \cdot & \cdot & -b_x & -b_y & b_z & \cdot & -\sqrt{3}b_x \\ \cdot & \cdot & \cdot & \cdot & \cdot & -\sqrt{3}b_y & \sqrt{3}b_x & \cdot \end{pmatrix} \tag{34}$$

is a block-diagonal matrix and $\mathbf{b} \equiv \mathbf{B}/|\mathbf{B}|$. Here and in subsequent matrices the dots represent zeros. The equation is solved by

$$\hat{\boldsymbol{\lambda}}(\mathbf{x}, t) = \sum_i \mathrm{e}^{-\omega(\mathbf{x})a_i t} P_i \cdot \hat{\boldsymbol{\lambda}}(\mathbf{x}, 0), \tag{35}$$

---

[6] Here we assume that the magnetic fields are static, but time-varying fields can also be modelled, as described in Petersen and Mølmer [34].

where $\omega(\mathbf{x}) = \mu_B g_F |\mathbf{B}(\mathbf{x})|$, $a_i, \mathbf{v}_i$ are the eigenvalues and eigenvectors of $\mathcal{A}$ with corresponding projectors $P_i \equiv \mathbf{v}_i \wedge \mathbf{v}_i$. The eigenvectors are imaginary integers $\{a\} = i\{-2, -1, -1, 0, 0, 1, 1, 2\}$, indicating the half-period behaviour of some $\hat{\mathbf{j}}$ variables. The macroscopic operators evolve as

$$\hat{\mathbf{\Lambda}}(t) = \int d^3x \, \rho_{at}(\mathbf{x}) \sum_i e^{-\omega(\mathbf{x})a_i t} P_i \cdot \hat{\mathbf{\lambda}}(\mathbf{x}, 0) \tag{36}$$

$$= \sum_i e^{-\omega_0 a_i t} \int d^3x \, \rho_{at}(\mathbf{x}) \, e^{-\tilde{\omega}(\mathbf{x})a_i t} P_i \cdot \hat{\mathbf{\lambda}}(\mathbf{x}, 0), \tag{37}$$

where $\omega(\mathbf{x}) = \omega_0 + \tilde{\omega}(\mathbf{x})$. We now assume that $\hat{\mathbf{\lambda}}(\mathbf{x}, 0)$ is uniform[7], so that the $\mathbf{x}$-dependent terms can be collected as $r_i(t) \equiv \int d^3x \, \rho_{at}(\mathbf{x}) \, e^{-\tilde{\omega}(\mathbf{x})a_i t}$. This gives

$$\hat{\mathbf{\Lambda}}(t) = \sum_i e^{-\omega_0 a_i t} r_i(t) P_i \cdot \hat{\mathbf{\Lambda}}(0)$$

$$= \mathcal{D}_\mathbf{B}(t) \cdot \mathcal{T}_\mathbf{B}(t) \cdot \hat{\mathbf{\Lambda}}(0), \tag{38}$$

where $\mathcal{T}_\mathbf{B}(t) = \sum_i e^{-\omega_0 a_i t} P_i$ describes the coherent evolution and $\mathcal{D}_\mathbf{B}(t) = \sum_i r_i(t) P_i$ describes the dephasing.

In many situations it is reasonable to assume a Lorentzian distribution for $\tilde{\omega}$. For example, in the highly elongated trap described below, we observe an atomic density $\rho(z)$ well approximated by a Lorentzian $\rho(z) = w/\pi(z^2 + w^2)$ where $w = 4.8$ mm is the full-width half-maximum (FWHM) extent of the ensemble. The decay term is then $r_i(t) = e^{-w\gamma|a_i \partial B_\parallel/\partial z|t}$ or $r_i(t) = e^{-t/T_i}$ with $1/T_i = w\gamma|a_i \partial B_\parallel/\partial z|$, and

$$\mathcal{D}_\mathbf{B}(t) = \sum_i e^{-t/T_i} P_i. \tag{39}$$

To preserve the uncertainty principle in the presence of the decay implied by equation (39), we must introduce a noise contribution $\mathbf{N}(t)$ to the covariance matrix [17]. The transformation due to evolution under an inhomogeneous field is thus

$$\Gamma_\mathbf{\Lambda}(t) = \mathcal{D}_\mathbf{B}(t) \cdot \mathcal{T}_\mathbf{B}(t) \cdot \Gamma_\mathbf{\Lambda}(0) \cdot \mathcal{T}_\mathbf{B}^T(t) \cdot \mathcal{D}_\mathbf{B}^T(t) + \mathcal{N}(t), \tag{40}$$

where the added noise obeys

$$\mathcal{N}_\mathbf{B}(t) \geqslant \left| i\mathbf{\Sigma}' - i\mathcal{D}_\mathbf{B}(t) \cdot \mathbf{\Sigma} \cdot \mathcal{D}_\mathbf{B}^T(t) \right|, \tag{41}$$

where $|\cdot|$ indicates the matrix absolute value and $i\Sigma_{ij} \equiv \langle [\hat{\Lambda}_i, \hat{\Lambda}_j] \rangle$ and $\mathbf{\Sigma}'$ are the commutation matrices before and after the transformation [35]. Absent an indication that the dephasing should be extra noisy, we take the equality sign in equation (41). We note that dephasing due to arbitrary field inhomogeneity can be included in the model by spatially partitioning the ensemble into subensembles with different local fields [17].

In addition to the dephasing of the atomic terms described above, the covariance matrix Γ undergoes a coherent evolution as described by equation (21) in terms of the matrix

$$\mathbf{T}_\mathbf{B}(t) = \begin{pmatrix} \mathbb{1}_{3\times3} & \cdot & \cdot \\ \gamma\mathcal{F}(t) & \gamma|\mathbf{B}(\mathbf{x})|\mathcal{A} & \cdot \\ \cdot & \cdot & \mathbb{1}_{3\times3} \end{pmatrix}, \tag{42}$$

---

[7] This assumption is clearly violated in some cases, for example in spin–echo experiments. However, it works remarkably well in many other situations.

where the matrix $\mathcal{A}$ is described above in equation (34) and

$$
\mathcal{F}_{\mathbf{B}}(t) \equiv \begin{pmatrix}
\cdot & F_z(t) & -F_y(t) \\
-F_z(t) & \cdot & F_x(t) \\
F_y(t) & -F_x(t) & \cdot \\
J_l(t) & J_k(t) & -2J_y(t) \\
-J_k(t) & J_l(t) & 2J_x(t) \\
J_y(t) & \sqrt{3}J_m(t) - J_x(t) & -J_l(t) \\
-\sqrt{3}J_m(t) - J_x(t) & -J_y(t) & J_k(t) \\
\sqrt{3}J_l(t) & -\sqrt{3}J_k(t) & \cdot
\end{pmatrix}.
\tag{43}
$$

Since the terms in $\mathcal{F}_{\mathbf{B}}(t)$ explicitly depend on the average atomic vector $\bar{\boldsymbol{\Lambda}}(t)$ at time t, we update the covariance matrix in small time steps $\tau \ll \omega_0$ and keep track of the $\Gamma(t)$ and $\bar{\mathbf{V}}(t)$ at each step. The covariance matrix finally evolves according to

$$
\Gamma(t+\tau) = \mathbf{D_B} \cdot \mathbf{T_B} \cdot \Gamma(t) \cdot [\mathbf{T_B}]^{\mathrm{T}} \cdot [\mathbf{D_B}]^{\mathrm{T}} + \mathbf{N_B},
\tag{44}
$$

where $\mathbf{D_B} \equiv \mathbb{1}_{3\times 3} \oplus \mathcal{D}_{\mathbf{B}} \oplus \mathbb{1}_{3\times 3}$ and $\mathbf{N_B} \equiv \mathbb{0}_{3\times 3} \oplus \mathcal{N}_{\mathbf{B}} \oplus \mathbb{0}_{3\times 3}$.

3.5. Combined effects

To combine the coherent rotations with decoherence, we follow Koschorreck and Mitchell [17] and apply alternately equations (17) and (21), equations (22) and (30) and equations (38) and (44) after subdividing the time interval into sufficiently small steps τ. Note that τ is typically much smaller during the optical pulses than in the time between them, but in both cases we continue to subdivide the time evolution until the results converge.

4. Measurement

After passing through the ensemble, the optical pulses are typically measured by balanced polarimetry. This allows one component $\hat{S}_{\mathrm{det}}^{(m)}$ of $\hat{\mathbf{S}}^{(m)}$ to be detected. In the process, the pulse is absorbed by the detector and any possible information about the other components of $\hat{\mathbf{S}}^{(m)}$ is lost. We can describe the projective measurement by a unit vector $\mathbf{p}^{(m)}$, defined such that $\mathbf{p}^{(m)} \cdot \hat{\mathbf{V}} = \hat{S}_{\mathrm{det}}^{(m)}$.

The result of the measurement is random and Gaussian-distributed, with a variance $\mathrm{var}(\hat{S}_{\mathrm{det}}) = \mathbf{p}^{(m)} \cdot \Gamma_{\mathbf{V}} \cdot \mathbf{p}^{(m)}$. The correlation of $\hat{S}_{\mathrm{det}}^{(m)}$ with other variables are given by the vector $\Gamma_{\mathbf{V}} \cdot \mathbf{p}^{(m)}$. Finally, we can calculate the post-measurement uncertainty in $\hat{\mathbf{V}}$, in light of the measurement result and the known correlations, to find the posterior uncertainty

$$
\begin{aligned}
\Gamma'_{\mathbf{V}} &= \Gamma_{\mathbf{V}} - \frac{(\Gamma_{\mathbf{V}} \cdot \mathbf{p}^{(m)}) \wedge (\Gamma_{\mathbf{V}} \cdot \mathbf{p}^{(m)})}{\mathbf{p}^{(m)} \cdot \Gamma_{\mathbf{V}} \cdot \mathbf{p}^{(m)}}, \\
&= \Gamma_{\mathbf{V}} - \Gamma_{\mathbf{V}} [\Pi_{\mathbf{p}^{(m)}} \Gamma_{\mathbf{V}} \Pi_{\mathbf{p}^{(m)}}]^{(\mathrm{MP})} \Gamma_{\mathbf{V}}^{\mathrm{T}}
\end{aligned}
\tag{45}
$$

where the superscript $^{(\mathrm{MP})}$ indicates the Moore–Penrose pseudo-inverse and $\Pi_{\mathbf{p}^{(m)}} = \mathbf{p}^{(m)} \wedge \mathbf{p}^{(m)}$ is a projector.

It should be noted that there is nothing stochastic in the simulation method: only the average values, variances and covariances are computed. This again relies on the assumption that the fluctuations remain within a linear regime.

5. Initial state and technical noise contributions

A variety of initial states can be used with this approach, subject to a few limitations: the average value $\bar{\mathbf{V}}$ must be physical, i.e. within the range of $\hat{\mathbf{V}}$ for N_A atoms and N_L photons. The Robertson–Schrödinger uncertainty principle

$$\delta A^2 \delta B^2 \geqslant \tfrac{1}{4} |\langle [A, B]\rangle|^2 \tag{46}$$

places lower limits on the uncertainty implied by $\Gamma_{\mathbf{V}}$. Given any two scalar operators $\hat{a} \equiv \mathbf{a} \cdot \hat{\mathbf{V}}$, $\hat{b} \equiv \mathbf{b} \cdot \hat{\mathbf{V}}$

$$\delta a^2 \delta b^2 = (\mathbf{a} \cdot \Gamma_{\mathbf{V}} \cdot \mathbf{a})(\mathbf{b} \cdot \Gamma_{\mathbf{V}} \cdot \mathbf{b}) \geqslant \tfrac{1}{4} \left| a_i b_j c_{\hat{V}_k}^{\hat{V}_i \hat{V}_j} \bar{v}_k \right|^2. \tag{47}$$

In many situations it is appropriate to assume an initial state of the form $R \equiv \rho^{\otimes N_A}$ for the atoms. For example, if optical pumping is used to initialize the state it is often reasonable to assume the atoms are independently pumped into a state ρ. This gives $\bar{\mathbf{\Lambda}} = N_A \mathrm{Tr}[\hat{\boldsymbol{\lambda}}\rho]$ and $\Gamma_{\mathbf{\Lambda}} = N_A \Gamma_{\boldsymbol{\lambda}}$. If ρ is a pure state, then R describes a coherent spin state (CSS).

We note an important subtlety about using CSSs for practical modelling: if ρ is a pure state, it is fully polarized along some spin direction $\boldsymbol{\lambda}_\rho$, with no uncertainty in that direction. This manifests as a zero eigenvalue of $\Gamma_{\boldsymbol{\lambda}}$, and, if we naively apply the above, also in $\Gamma_{\mathbf{\Lambda}}$. This is unrealistic, however. In practice, N_A is usually determined by a physical process with significant uncertainty, e.g. trap loading. Indeed, δN_A^2 is often larger than the quantum variances $N_A \Gamma_{\boldsymbol{\lambda}} \sim N_A$. This contributes a significant 'atomic technical noise' to $\Gamma_{\mathbf{\Lambda}}$. As shown in appendix B, for a state of the form $R = \rho^{\otimes N_A}$, where N_A has average $\bar{N}_A$ and variance δN_A^2,

$$\Gamma_{\mathbf{\Lambda}} = \bar{N}_A \Gamma_{\boldsymbol{\lambda}} + \delta N_A^2 (\bar{\boldsymbol{\lambda}} \wedge \bar{\boldsymbol{\lambda}}). \tag{48}$$

In most situations of interest the input light state is a coherent state. For example, in the experiments described below, we use an $\hat{S}_x$-polarized input, i.e. $\bar{\mathbf{S}} = (N_L/2, 0, 0)$, which has a covariance matrix $\Gamma_{\mathbf{S}} = \mathrm{diag}(N_L/4, N_L/4, N_L/4)$. The input average magnetic field components $\bar{\mathbf{B}}$ and covariance matrix $\Gamma_{\mathbf{B}}$ will depend on the modelled experiment.

In the experiments described below the atoms and light are independently initialized, and we assume that the atom, light and magnetic field variables are initially uncorrelated. Thus the initial covariance matrix of equation (9) can be written:

$$\Gamma_{\mathbf{V}} = \Gamma_{\mathbf{B}} \oplus \Gamma_{\mathbf{\Lambda}} \oplus \Gamma_{\mathbf{S}}. \tag{49}$$

6. An example: free-induction decay of collective atomic spin

We illustrate the formalism described above with a simple example. We study, experimentally and theoretically, a paramagnetic Faraday rotation measurement of the free-induction decay (FID) of input $\hat{F}_z$ and $\hat{F}_y$-polarized CSS precessing in a magnetic field. As described in Behbood *et al* [36], neglecting tensorial light shifts described by the G_2 term of equation (10), this leads

to a measurable polarization rotation angle

$$\langle\phi(t)\rangle = \frac{G_1}{|B|^2} \times \begin{cases} \left[B_y B_z \left(1 - \cos(\gamma|B|t)\,\mathrm{e}^{-t/T} \right) + B_x |B| \sin(\gamma B t)\,\mathrm{e}^{-t/T} \right] \langle \hat{F}_y(0) \rangle \\ \left[B_z^2 + [B_x^2 + B_y^2] \cos(\gamma|B|t)\,\mathrm{e}^{-t/T} \right] \langle \hat{F}_z(0) \rangle \end{cases} \tag{50}$$

for the input $\hat{F}_z$ and $\hat{F}_y$-polarized CSS, respectively. The transverse relaxation time $T = 1/(w\gamma|B'_\parallel|)$ is due to the field-parallel gradient component $B'_\parallel \equiv \partial|B|/\partial_z$, and a Lorentzian distribution (FWHM w) of atoms along z, the trap axis, as described in appendix C. Tensorial light shifts induce an additional nonlinear rotation of the atomic spins, as described in Smith *et al* [20] and Deutsch and Jessen [31]. This measurement can be used to estimate an unknown vector magnetic field, as in Behbood *et al* [36], and is the basis of a proposal to prepare a planar-squeezed atomic spin state [37].

Our experimental apparatus, illustrated in figure 2, has been described in detail elsewhere [8, 25, 38, 39]. In brief, we work with an ensemble of up to one million ^{87}Rb atoms held in a weakly focused single beam optical dipole trap and probed by μs duration pulses of near-resonant light propagating along the trap axis and focused to a spot matching the radial width of the atomic cloud. This geometry produces a strong atom–light coupling, characterized by the effective on-resonance optical depth $d_0 \equiv (\sigma_0/A)N_A$, where σ_0 is the effective on–resonance scattering cross-section, A is an effective atom–light interaction area and N_A is the number of atoms [39]. In this experiment we observe an effective optical depth $d_0 = 29.0(2)$. The optical readout can achieve projection-noise-limited sensitivity, calibrated against a thermal spin state [38], and using dynamical decoupling techniques [25] has been used to demonstrate spin squeezing and entanglement-enhanced measurement sensitivity of the collective atomic spin [8].

For the FID measurement the atoms are initially polarized via optical pumping with a 5 μs duration pulse of circularly polarized light tuned to the $f = 1 \rightarrow f' = 1$ transition of the D$_2$ line. The optical pumping pulse propagates either along the trap axis to produce an F_z-polarized CSS ($\langle \hat{F}_z(0) \rangle = N_A$), or perpendicular to the trap to produce an F_y-polarized CSS ($\langle \hat{F}_y(0) \rangle = N_A$). Simultaneously with the optical pumping pulse, light tuned to the $f = 2 \rightarrow f' = 2$ transition of the D$_2$ line is applied to prevent atoms collecting in the $f = 2$ hyperfine state. This ensures that we prepare the initial CSS with good fidelity. We estimate an optical pumping efficiency of $> 99\%$ for both the $\hat{F}_z$-polarized and $\hat{F}_y$-polarized CSSs. The remaining unpolarized atoms make a negligible contribution to the observed var(ϕ).

The atoms are then probed with a sequence of 1 μs long pulses of linearly polarized light ($\langle \hat{S}_x^{(\mathrm{in})} \rangle = \pm N_L/2$) detuned about 1 GHz from resonance with the $f = 1 \rightarrow f' = 0$ transition on the D$_2$ line and propagating along the trap axis. After each pulse, the Faraday rotation signal $\phi = \hat{S}_y^{(\mathrm{out})}/\hat{S}_x^{(\mathrm{in})}$ is recorded by a shot-noise limited polarimeter [40]. The pulses are either (a) all h–polarized and sent through the atoms at $P_1 = 10\,\mu$s intervals, or (b) pairs of alternately h- and v-polarized pulses separated by 3 μs and sent through the atoms $P_2 = 20\,\mu$s intervals. The entire experimental sequence is repeated up to 400 times to collect statistics.

Typical experimental data are shown in figure 2; we plot the evolution of the average signal $\bar{\phi}$ for an input $\hat{F}_y$– and $\hat{F}_z$–polarized CSS, and the evolution of the variance var(ϕ) for the same input states. The observed signal initially oscillates at the Larmor precession frequency $\omega_0 = 2\pi \times 9.2\,$kHz with an exponential decay, as described by equation (50). On top of this there is a collapse and revival of the oscillations driven by tensorial light shifts, as described in Smith *et al* [20] and Deutsch and Jessen [31], which rotate population out of
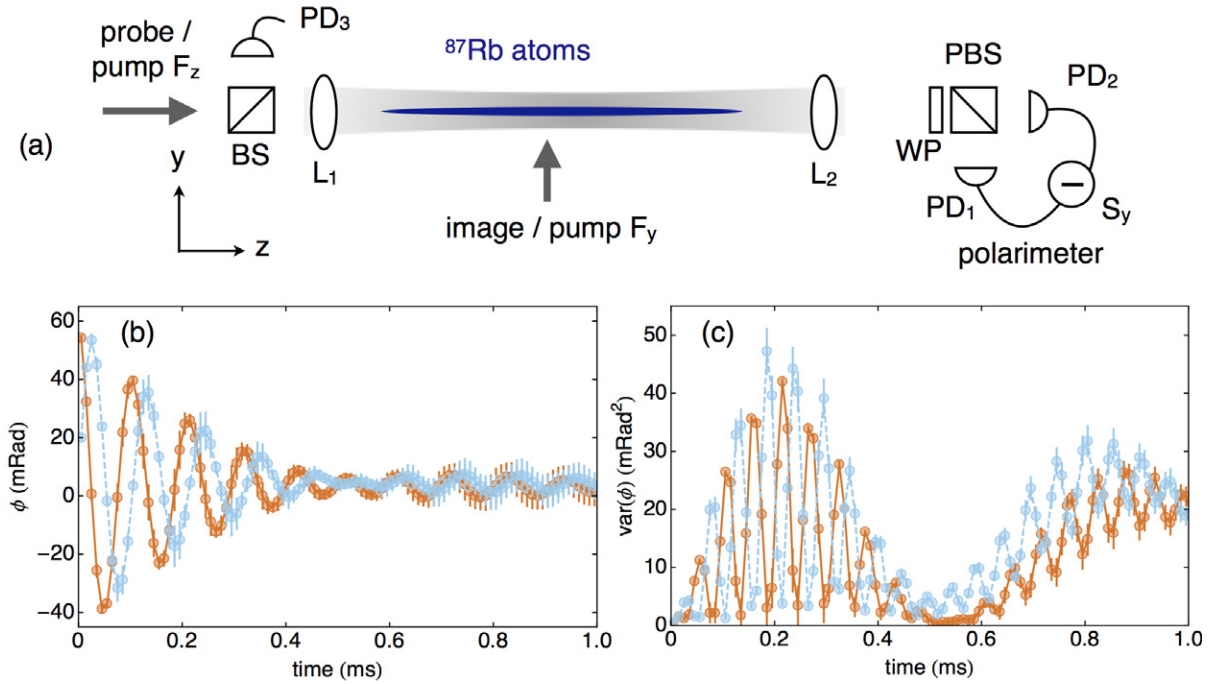
Figure 2. (a) Experimental setup. PD: photodiode; L: lens; WP: wave plate; BS: beam splitter; PBS: polarizing beam splitter. Atoms are loaded into a single-beam optical dipole trap and probed with pulses of light propagating along the trap axis. An external magnetic field is applied to coherently rotate the atomic spins, and gradient field components $\partial B_i / \partial z$ are actively cancelled. The initial atomic state is prepared via optical pumping with circularly polarized light either propagating perpendicular to or along the trap axis, to prepare an $\hat{F}_y$-polarized or $\hat{F}_z$-polarized CSS, respectively. Also shown are experimental data of (b) the average signal $\bar{\phi}$ for an input $\hat{F}_y$—and $\hat{F}_z$—polarized CSS (blue and orange, respectively), and (c) the evolution of the variance var(ϕ) for the same input states. Error bars represent $\pm 1\sigma$ statistical errors. The lines connect experimental points to aid visualization.

$\hat{F}_z$ and into the alignment variables $\hat{J}_{x,y}$ at a rate $\omega_{G_2} = (G_2 S_x / 2)(1/P_1) = 2\pi \times 0.43$ kHz. The revival is accompanied by a π phase shift in the oscillations (see figure 3 below for an illustration of this effect). The observed variance var(ϕ) oscillates at a frequency $2\omega_0$ and undergoes a similar but much more pronounced collapse and revival driven by the tensorial light shifts. Note that the observed variance in this experiment is dominated by technical noise; for our experimental parameters, the quantum noise contributions from both the atomic and light variables are $\ll 1$ mrad^2. The dominant technical noise contributions are due to uncertainty in the atom number δN_A^2, and magnetic field noise, described by the covariance matrix Γ_B, coupled into the observed variable via tensorial light shifts. We illustrate the effect of these terms separately in figure 3, by running numerical simulations, as described in detail in section 7, using experimental parameters from the data shown in figure 2 and setting variously the Γ_B, δN^2 and G_2 terms equal to zero.
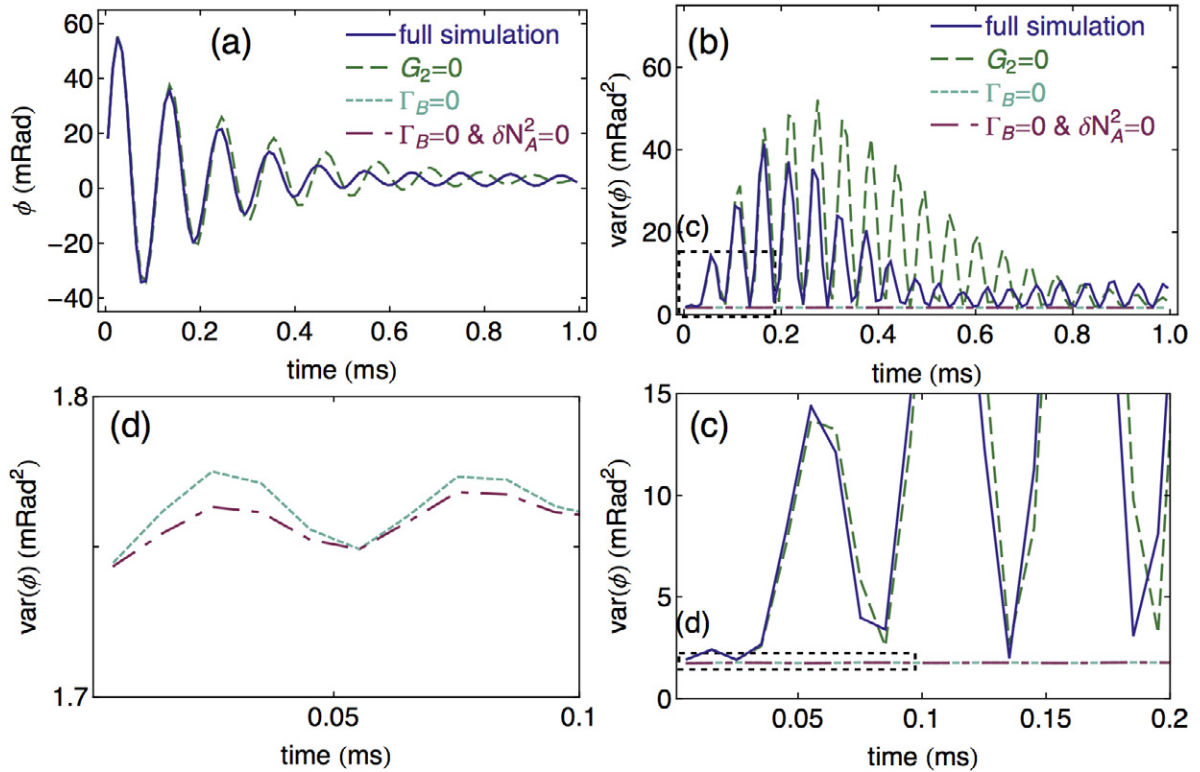
Figure 3. Theoretical curves illustrating the effect of technical noise terms and tensorial light shifts on the mean $\bar{\phi}$ and variance $\text{var}(\phi)$ of the observed signal. (a) Tensorial light shifts rotate population out of $\hat{F}_z$ and into the alignment variables $\hat{J}_{x,y}$ leading to a collapse and revival of the mean $\bar{\phi}$. The revival is accompanied by a π phase shift in the oscillations, as is evident in the simulation with $G_2 = 0$, which removes the effect of tensorial light shifts. (b)–(d) The observed variance $\text{var}(\phi)$ undergoes a more pronounced collapse and revival driven by the tensorial light shifts, which couple technical noise from the atomic variables $\hat{\boldsymbol{\Lambda}}$ and the magnetic field covariance matrix $\Gamma_{\mathbf{B}}$ into the observed variable. The contribution to the observed signal in (b) is due to magnetic field noise. Technical noise in the atomic variables due to uncertainty δN_A^2 in the atom number only adds significant noise only during the early stages of the evolution. This is illustrated more clearly in the magnified plots (c) and (d). The dot-dashed magenta line in plot (d) illustrates the quantum noise contributions due to the light (shot-noise) and atoms (projection-noise).

7. Simulation of free-induction decay

In order to simulate the FID experiment, we need to estimate a number of experimental parameters, including the input state vector $\bar{\mathbf{V}}$ and covariance matrix $\Gamma_{\mathbf{V}}$, the coupling constants of equation (10) and the decoherence terms in equations (26)–(29) and (39). The atom–light coupling constant G_1 is calibrated in an auxiliary experiment as described in Kubasik *et al* [39]. From this calibration we calculate the effective atom–light interaction area A, the coupling

constant G_2 of equation (10) and the single-photon scattering probability η_γ used to describe the optically induced decoherence terms in equations (26)–(29) (see [41] for details).

We estimate the average magnetic field $\bar{\mathbf{B}}$ for a single experimental data set by fitting the observed signal $\langle \phi(t) \rangle$ with equation (50), as described detail in Behbood *et al* [36]. Since equation (50) neglects the effect of tensorial light shifts, we fit only the first $250\,\mu$s of each measured signal to minimize the systematic error that this approximation introduces. From the fits we also determine the coherence time T that is used in equation (39) From the same fits we estimate the number of atoms $\langle \hat{F}_i(0) \rangle = N_A/2$. Assuming an input state of the form $R \equiv \rho_{\hat{f}_i}^{\otimes N_A}$ for the atoms, this specifies the initial atomic state via $\bar{\mathbf{\Lambda}} = N_A \text{Tr}[\hat{\mathbf{\lambda}} \rho_{\hat{f}_i}]$. The number of photons N_L in each pulse is independently measured via a reference detector, as shown in figure 2. Together, these estimates specify the initial state of the vector $\bar{\mathbf{V}}$.

Statistics from the fits to equation (50) across the data set allow us to estimate the covariance matrix $\Gamma_{\mathbf{B}}$. Similarly, we estimate the uncertainty δN_A^2 in the atom number from $\text{var}(\hat{F}_i) = \text{var}(N_A/2)$ (which includes contributions from variable trap loading and state preparation efficiency as well as measurement uncertainty). This allows us to estimate the initial covariance matrix $\Gamma_{\mathbf{\Lambda}}$ using equation (48). Since the measurement is shot-noise limited, the input light covariance matrix is $\Gamma_{\mathbf{S}} = (N_L/4, N_L/4, N_L/4)$. Together, via equation (49), these specify the initial covariance matrix $\Gamma_{\mathbf{V}}(0)$.

As an example, we give the experimental parameters in detail of the first example described in section 6, shown in figures 2(b) and (c). For this experiment, we set the detuning of the probe to $\Delta = -700\,$MHz and probe with a sequence of $1\,\mu$s long h-polarized pulses of light with on average $N_L = 7.19 \times 10^6$ photons per pulse at $10\,\mu$s intervals. The measured average magnetic field was $\mathbf{B} = (11.92, -4.08, -3.23)\,$mG, with a covariance matrix

$$\Gamma_{\mathbf{B}} = \begin{pmatrix} 0.091 & 0.005 & -0.023 \\ 0.005 & 0.116 & 0.010 \\ -0.023 & 0.011 & 0.007 \end{pmatrix} \text{mG}^2. \tag{51}$$

We estimate $N_A = 6.05 \times 10^5$ and $\Delta N_A = 1.6 \times 10^3$, giving an initial atomic vector for the $\hat{F}_y$–polarized input $\mathbf{\Lambda}(t = 0) = (0, 1, 0, -0.5, 0, 0, 0, -0.29) \times N_A$ and covariance matrix

$$\Gamma_{\mathbf{\Lambda}}(t = 0) = \begin{pmatrix} 0.5 & 0 & 0 & 0 & 0.5 & 0 & 0 & 0 \\ 0 & 4.98 & 0 & -2.49 & 0 & 0 & 0 & -1.43 \\ 0 & 0 & 0.5 & 0 & 0 & 0 & 0.5 & 0 \\ 0 & -2.49 & 0 & 1.49 & 0 & 0 & 0 & 0.28 \\ 0.5 & 0 & 0 & 0 & 0.5 & 0 & 0 & 0 \\ 0 & 0 & 0 & 0 & 0 & 1 & 0 & 0 \\ 0 & 0 & 0.5 & 0 & 0 & 0 & 0.5 & 0 \\ 0 & -1.43 & 0 & 0.28 & 0 & 0 & 0 & 1.16 \end{pmatrix} \times N_A. \tag{52}$$

We further estimate a coherence time $T = 450 \pm 10\,\mu$s. The calibrated coupling constants were $G_1 = 1.8 \pm 0.2 \times 10^{-7}\,$rad atom^{-1} and $G_2 = -9.3 \pm 0.8 \times 10^{-9}\,$rad atom^{-1}, and the atom–light scattering parameter $\eta_\gamma = 1.1 \times 10^{-9}$.

Together these parameters determine the initial state vector $\bar{\mathbf{V}}(t=0)$ and covariance matrix $\Gamma_{\mathbf{V}}(t=0)$ as described in section 5, the atom–light coupling constants of equation (10), the magnetic field components of equation (33), and the decoherence terms in equations (26)–(29) and equation (39). With these input parameters, we then run numerical simulations of the evolution of the state vector $\bar{\mathbf{V}}$ and covariance matrix $\Gamma_{\mathbf{V}}$ following the procedure described in section 3, keeping track of $\mathbf{V}(t_m)$ and $\Gamma_{\mathbf{V}}(t_m)$ at each time step. As in the experiment, we alternate between a time interval of $1\,\mu s$ in which the light is present and an interval of $9\,\mu s$ with no light present. For the numerical calculations, we divide these intervals into 50 and 100 sub-steps, respectively, which is sufficient to ensure numerical convergence of the results. The results of the simulations (dark blue curves) are plotted along with the experimental data (light blue circles) in figures 4(a) and (b) for both the mean $\bar{\phi}$ and variance var(ϕ) with an input $\hat{F}_y$-polarized atomic state.

We observe excellent qualitative and quantitative agreement between the simulations and the observed mean $\bar{\phi}$ and variance var(ϕ) in the rotation angle with no further free parameters adjusted in the calculations. For the mean $\bar{\phi}$, we reproduce the observed behaviour in our simulations over the entire 1 ms of observation, as shown in figures 4(b) and (d). For the variance var(ϕ) the quantitative agreement is initially good, but breaks down at longer times. This can be explained by the effect of the uncertainty in the magnetic field, described by the covariance matrix $\Gamma_{\mathbf{B}}$, which eventually drives the atomic variables out of the Gaussian approximation.

Because magnetic precession is cyclic, not linear, an initially Gaussian spin distribution will become non-Gaussian due to uncertainty in the precession frequency. As some parts of the distribution precess faster than others, the distribution begins to 'wrap around' the Bloch sphere, forcing a non-Gaussian shape on the distribution. It is convenient to define a time $\tau_{\text{gauss}} \equiv \pi/(\gamma_F \Delta B_\parallel)$, where $\Delta B_\parallel$ is the uncertainty in $\mathbf{B}$ along the average field direction, found using $\Gamma_{\mathbf{B}}$ of equation (51). τ_{gauss} indicates the moment at which the precession angle uncertainty becomes π. Perhaps surprisingly, the observed and predicted variances (see figures 2(c) and (e)) agree very well up to nearly $t = \tau_{\text{gauss}} \approx 0.45$ ms, showing that the theory gives accurate results even for significant departures from Gaussianity. The agreement in the *average* values persists even for $t > \tau_{\text{gauss}}$. This changes accumulates with time and becomes much more significant than the technical noise in the number of atoms so that while the atomic noise is important early on, the dephasing effect of magnetic field inhomogeneities becomes the dominant contribution for larger times.

The collapse and revival of the oscillations in figures 4(a) and (b) is due to rotations driven by the tensorial light shift. The effect of the tensorial light shifts can be reduced either by probing further off resonance, or by probing the atoms alternately with h– and v–polarized pulses, as described in detail in [38]. We illustrate this in figures 4(c)–(d), where we compare these data to FID measurements (and simulations) made with two alternate probing strategies. In figures 4(c) and (d) we set the detuning to $\Delta = -1.5$ GHz and repeat the single–polarization probing sequence. In figures 4(e) and (f) we set the detuning to $\Delta = -700$ MHz and probe with pairs of alternately h- and v-polarized pulses separated by $3\,\mu s$ are sent through the atoms $20\,\mu s$ intervals (for clarity we plot only the h–polarized pulses). This results in the same total number of photons used per unit time as in the single polarization probing strategy. With these data we observe similar behaviour in the mean $\bar{\phi}$ and variance var(ϕ) at both detunings, indicating the effective cancellation of tensorial light shifts in these experiments. We also observe non-zero minima in var(ϕ) at all phases in the experimental data for $t > 0.5$ ms, which are not reproduced in our calculations. Looking at the data globally, we also note that lower envelope rises more
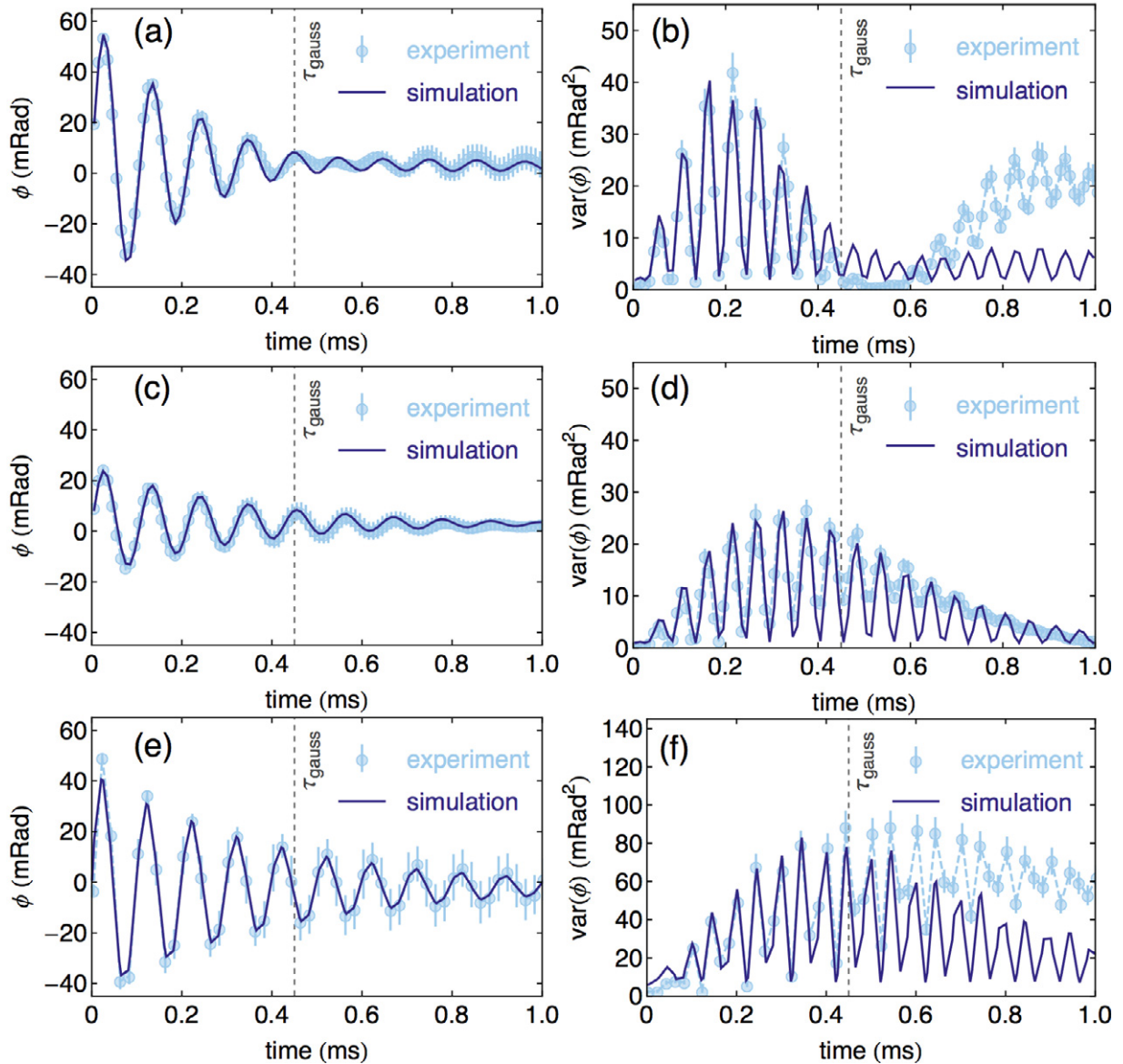
Figure 4. Comparison of experimental data (light blue circles) with numerical simulations (dark blue curves) of the mean $\bar{\phi}$ (a), (c) and (e) and variance var(ϕ) (b), (d) and (f) of the optical rotation of the probing light. For (a) and (b) we set the detuning of the probe to $\Delta = -700$ MHz and probed the atoms with a sequence of $1\,\mu$s long h–polarized pulses of light with on average $N_L = 7.19 \times 10^6$ photons per pulse at $10\,\mu$s intervals. For (c) and (d) we set the detuning of the probe to $\Delta = -1.5$ GHz and probed with the same measurement sequence with on average $N_L = 1.35 \times 10^7$ photons per pulse. For (e) and (f) we set the detuning of the probe to $\Delta = -700$ MHz and probed the atoms with a sequence pairs of $1\,\mu$s long pulses with alternating h– and v–polarization, separated by $3\,\mu$s and sent through the atoms $20\,\mu$s intervals with on average $N_L = 2.10 \times 10^6$ photons per pulse. Error bars represent $\pm 1\sigma$ statistical errors. See text for details.

in the data than in the simulation. This may due to the curvature of the Bloch sphere: for small uncertainty in precession angle $\Delta\theta = t\gamma_F\Delta B_\parallel$, we will have $\Delta F_z \propto \Delta\theta\,\partial_\theta F_z$. For flat parts of the curve $F_z(\theta)$ there will be zero $\partial_\theta F_z$ and thus zero ΔF_z but for larger $\Delta\theta$, we need to take into account higher derivatives, i.e. the curvature $\partial_\theta^2 F_z$ and higher. This implies a first-order insensitivity of the measured component to rotations, and thus (to first order) zero contribution to the measured $\Delta\theta$. When the distribution describing the state 'wraps around' the Bloch sphere, the second-order effects, which are not taken into account in the Gaussian approximation, become important and give a contribution to the measured variance proportional to $\delta\mathbf{B}^2$. This contribution is necessarily positive, and raises the lower envelope above the level predicted by the simulations.

8. Conclusions

We have presented a method for describing the quantum dynamics of spin-1 atomic ensembles, extending the method introduced for quantum light interfaces [13, 15, 16], developed for spin-1/2 atomic ensembles by Madsen and Mølmer [14] and generalized by Koschorreck *et al* [17] and Toth *et al* [42]. Our approach, which explicitly includes the so-called 'spin alignment' degrees of freedom, fits naturally with the light–matter interaction, which couples both spin alignment and spin orientation to the optical Stokes parameters. For spin-1 our description is complete within the Gaussian approximation, while for larger spins it is still useful when octopole and higher spin moments can be neglected. We also include the important technical noise associated with magnetic fields and noise due to uncertain atom number, as typically arises due to stochastic trap-loading processes. Finally, we give explicit formulae for the noise introduced by spontaneous scattering during the optical probing process and due to dephasing in an inhomogeneous magnetic field.

We have tested the model against experiment in a scenario involving all of these effects. We compute the evolution of the spin orientation average and variance for atomic ensembles with uncertain atom number, undergoing a combination of free-induction decay and alignment-to-orientation conversion in the presence of a noisy magnetic field. The simulation is compared to experimental observations made with a cold ^{87}Rb ensemble held in an optical dipole trap, probed by shot-noise-limited Faraday rotation with near-resonant light. We find good agreement within the Gaussian regime. In addition to validating the model, the experiments provide a heuristic guide to the limits of the Gaussian approximation in these systems.

Given that most atomic ensemble experiments are performed with spin-1 or larger atoms, the technique described here will allow more accurate modelling of established quantum optical protocols, e.g. quantum memory [15], quantum non-demolition measurement [26, 38], dynamical decoupling [25], spin squeezing [8] and vector magnetometry [36], as well as proposed applications such as generation of macroscopic singlet states [42, 43] and planar squeezed states [37].

Acknowledgments

Appendix A. Proof of equations (23) and (24)

For brevity, we write the covariance as

$$\mathcal{C}(\mathbf{A}, \mathbf{B}) \equiv \tfrac{1}{2}\langle \mathbf{A} \wedge \mathbf{B} + (\mathbf{B} \wedge \mathbf{A})\rangle - \langle \mathbf{A}\rangle \wedge \langle \mathbf{B}\rangle, \tag{A.1}$$

where the expectation is taken on the state of the ensemble. In this notation, $\Gamma_{\mathbf{\Lambda}} \equiv \mathcal{C}(\hat{\mathbf{\Lambda}}, \hat{\mathbf{\Lambda}})$ where as above $\hat{\mathbf{\Lambda}} = \sum_i \hat{\mathbf{\lambda}}^{(i)}$. We assume that all atoms are statistically equivalent, so that $\langle \hat{\mathbf{\lambda}}^{(i)} \wedge \hat{\mathbf{\lambda}}^{(j)}\rangle = \langle \hat{\mathbf{\lambda}}^{(1)} \wedge \hat{\mathbf{\lambda}}^{(2)}\rangle$ for all $i \neq j$ and $\langle \hat{\mathbf{\lambda}}^{(i)} \wedge \hat{\mathbf{\lambda}}^{(i)}\rangle = \langle \hat{\mathbf{\lambda}}^{(1)} \wedge \hat{\mathbf{\lambda}}^{(1)}\rangle$ for all i. We then have

$$\Gamma_{\mathbf{\Lambda}} = \sum_{i,j} \mathcal{C}(\hat{\mathbf{\lambda}}^{(i)}, \hat{\mathbf{\lambda}}^{(j)}) = N_{\mathrm{A}}\mathcal{C}(\hat{\mathbf{\lambda}}^{(1)}, \hat{\mathbf{\lambda}}^{(1)}) + N_{\mathrm{A}}(N_{\mathrm{A}} - 1)\mathcal{C}(\hat{\mathbf{\lambda}}^{(1)}, \hat{\mathbf{\lambda}}^{(2)}), \tag{A.2}$$

which we solve for $\mathcal{C}(\hat{\mathbf{\lambda}}^{(1)}, \hat{\mathbf{\lambda}}^{(2)})$ to get

$$\mathcal{C}(\hat{\mathbf{\lambda}}^{(1)}, \hat{\mathbf{\lambda}}^{(2)}) = \frac{\Gamma_{\mathbf{\Lambda}} - N_{\mathrm{A}}\mathcal{C}(\hat{\mathbf{\lambda}}^{(1)}, \hat{\mathbf{\lambda}}^{(1)})}{N_{\mathrm{A}}(N_{\mathrm{A}} - 1)}. \tag{A.3}$$

Because of the symmetry, removing atoms does not change $\mathcal{C}(\hat{\mathbf{\lambda}}^{(1)}, \hat{\mathbf{\lambda}}^{(1)})$ or $\mathcal{C}(\hat{\mathbf{\lambda}}^{(1)}, \hat{\mathbf{\lambda}}^{(2)})$. If a fraction $1 - \mathcal{X}$ of the atoms is removed, the covariance matrix $\Gamma_{\mathbf{\Lambda}}^{(\mathcal{X}N_{\mathrm{A}})}$ of the remaining atoms can be calculated as in equation (A.2), but summing i and j from 1 to $\mathcal{X}N_{\mathrm{A}}$. We find

$$\begin{aligned}
\Gamma_{\mathbf{\Lambda}}^{(\mathcal{X}N_{\mathrm{A}})} &= \mathcal{X}N_{\mathrm{A}}\mathcal{C}(\hat{\mathbf{\lambda}}^{(1)}, \hat{\mathbf{\lambda}}^{(1)}) + \mathcal{X}N_{\mathrm{A}}(\mathcal{X}N_{\mathrm{A}} - 1)\mathcal{C}(\hat{\mathbf{\lambda}}^{(1)}, \hat{\mathbf{\lambda}}^{(2)}) \\
&= \Gamma_{\mathbf{\Lambda}}^{(N_{\mathrm{A}})}\frac{\mathcal{X}(\mathcal{X}N_{\mathrm{A}} - 1)}{N_{\mathrm{A}} - 1} + \Gamma_{\lambda}\left(\frac{\mathcal{X}(1 - \mathcal{X})N_{\mathrm{A}}^2}{N_{\mathrm{A}} - 1}\right),
\end{aligned}$$

where

$$\Gamma_{\lambda} \equiv \mathcal{C}(\hat{\mathbf{\lambda}}^{(1)}, \hat{\mathbf{\lambda}}^{(1)}) \tag{A.4}$$

is the single-atom covariance matrix. Dropping terms of order $1/N_{\mathrm{A}}$ and smaller,

$$\Gamma_{\mathbf{\Lambda}}^{(\mathcal{X}N_{\mathrm{A}})} = \Gamma_{\mathbf{\Lambda}}^{(N_{\mathrm{A}})}\mathcal{X}^2 + \Gamma_{\lambda}\mathcal{X}(1 - \mathcal{X})N_{\mathrm{A}}. \tag{A.5}$$

This accounts for the change in $\Gamma_{\mathbf{\Lambda}}$ due to removing $(1 - \mathcal{X})N_{\mathrm{A}}$ atoms. We must also account for the noise of returning a fraction p of these atoms to the ensemble in a decohered state. We assume they are completely random, and thus add the noise of a thermal state (i.e. variance $f(f+1)/3$ per atom).

$$\Gamma_{\mathbf{\Lambda}}^{(\mathcal{X}N_{\mathrm{A}})} = \Gamma_{\mathbf{\Lambda}}^{(N_{\mathrm{A}})}\mathcal{X}^2 + \Gamma_{\lambda}\mathcal{X}(1 - \mathcal{X})N_{\mathrm{A}} + 2p(1 - \mathcal{X})N_{\mathrm{A}}\mathbb{1}/3. \tag{A.6}$$

Here

$$\begin{aligned}
\Gamma_{\lambda} &= \tfrac{2}{3}\mathbb{1}_{8\times 8} - \bar{\mathbf{\lambda}} \wedge \bar{\mathbf{\lambda}} + \sum_k \bar{\lambda}_k \mathbf{M}^{(k)}, \\
M_{ij}^{(k)} &\equiv \tfrac{1}{4}\mathrm{Tr}[\hat{\lambda}_k\{\hat{\lambda}_i, \hat{\lambda}_j\}],
\end{aligned} \tag{A.7}$$

where $\{\cdot, \cdot\}$ indicates the anti-commutator. This can be shown using the expectation $\mathrm{Tr}[\rho\hat{\lambda}_i] = \bar{\lambda}_i$ and the orthonormality condition $\mathrm{Tr}[\lambda_i\lambda_j] = 2\delta_{ij}$ from which $\mathrm{Tr}[\{\lambda_i, \lambda_j\}] = 4\delta_{ij}$. We find the single-particle state $\rho = \tfrac{1}{3}\mathbb{1} + \tfrac{1}{2}\sum_i \bar{\lambda}_i\hat{\lambda}_i$ and the covariances

$$\begin{aligned}
\mathrm{cov}(\lambda_i, \lambda_j) &\equiv \tfrac{1}{2}\langle\{\hat{\lambda}_i, \hat{\lambda}_j\}\rangle - \langle\hat{\lambda}_i\rangle\langle\hat{\lambda}_j\rangle \\
&= \tfrac{2}{3}\delta_{i,j} + \tfrac{1}{4}\sum_k \bar{\lambda}_k\mathrm{Tr}[\hat{\lambda}_k\{\hat{\lambda}_i, \hat{\lambda}_j\}] - \bar{\lambda}_i\bar{\lambda}_j.
\end{aligned} \tag{A.8}$$

Appendix B. Noise from uncertain atom number

We consider the statistics of $\hat{\boldsymbol{\Lambda}}$ for ensembles with N_A atoms in a permutationally invariant product state $R^{(N_A)} = \rho^{\otimes N_A}$, and taking a statistical average over N_A. We indicate averages with subscripts, e.g. $\langle \hat{\boldsymbol{\Lambda}} \rangle_R = \text{Tr}[\hat{\boldsymbol{\Lambda}} R]$ indicates an expectation with respect to the state R, while $\langle \hat{\boldsymbol{\Lambda}} \rangle_{R,N_A} = \langle \text{Tr}[\hat{\boldsymbol{\Lambda}} R^{(N_A)}] \rangle_{N_A}$ indicates a statistical average of $\langle \hat{\boldsymbol{\Lambda}} \rangle_R$ over the distribution of N_A. Due to the structure of $R^{(N_A)}$, $\langle \hat{\boldsymbol{\lambda}}^{(k)} \rangle_{R^{(N_A)}} = \langle \hat{\boldsymbol{\lambda}}^{(1)} \rangle_\rho \equiv \langle \hat{\boldsymbol{\lambda}} \rangle_\rho$ is independent of both k and of N_A, so that

$$
\begin{aligned}
\langle \hat{\Lambda}_i \hat{\Lambda}_j \rangle_R &= \sum_{k,l=1}^{N_A} \langle \hat{\lambda}_i^{(k)} \hat{\lambda}_j^{(l)} \rangle_\rho \\
&= N_A \langle \hat{\lambda}_i \hat{\lambda}_j \rangle_\rho + N_A(N_A - 1) \langle \hat{\lambda}_i \rangle_\rho \langle \hat{\lambda}_j \rangle_\rho,
\end{aligned}
\tag{B.1}
$$

and thus

$$
\langle \hat{\Lambda}_i \hat{\Lambda}_j \rangle_{R,N_A} = \bar{N}_A \langle \hat{\lambda}_i \hat{\lambda}_j \rangle_\rho + (\delta N_A^2 + \bar{N}_A^2 - \bar{N}_A) \langle \hat{\lambda}_i \rangle_\rho \langle \hat{\lambda}_j \rangle_\rho,
\tag{B.2}
$$

where $\delta N_A^2 \equiv \langle N_A^2 \rangle - \langle N_A \rangle^2$ indicates the variance. At the same time

$$
\langle \hat{\Lambda}_i \rangle_{R,N_A} = \bar{N}_A \langle \hat{\lambda}_i \rangle_\rho,
\tag{B.3}
$$

so that

$$
\text{cov}(\hat{\Lambda}_i, \hat{\Lambda}_j)_{R,N_A} \equiv \tfrac{1}{2} \langle \hat{\Lambda}_i \hat{\Lambda}_j + \hat{\Lambda}_j \hat{\Lambda}_i \rangle_{R,N_A} - \langle \hat{\Lambda}_i \rangle_{R,N_A} \langle \hat{\Lambda}_j \rangle_{R,N_A}
\tag{B.4}
$$

$$
= \bar{N}_A \text{cov}(\hat{\lambda}_i, \hat{\lambda}_j)_\rho + \delta N_A^2 \langle \hat{\lambda}_i \rangle_\rho \langle \hat{\lambda}_j \rangle_\rho.
\tag{B.5}
$$

In terms of the single-atom covariance matrix Γ_λ of equation (A.4),

$$
\Gamma = \bar{N}_A \Gamma_\lambda + \delta N_A^2 (\bar{\boldsymbol{\lambda}} \wedge \bar{\boldsymbol{\lambda}}).
\tag{B.6}
$$

Appendix C. Inhomogeneous magnetic fields

The microscopic spin operators evolve as

$$
\mathbf{f}^i(t) = R(z_i, t) \mathbf{f}^i(0),
\tag{C.1}
$$

where $\mathbf{f}^i$ is the spin of the ith atom with position z_i and

$$
R(z, t) = \exp[\gamma_F t |\mathbf{B}(z)| A_B],
\tag{C.2}
$$

where

$$
A_B \equiv \begin{pmatrix} 0 & -\hat{B}_z & \hat{B}_y \\ \hat{B}_z & 0 & -\hat{B}_x \\ -\hat{B}_y & \hat{B}_x & 0 \end{pmatrix}
\tag{C.3}
$$

is the generator of rotations about $\mathbf{B}$ and $\hat{\mathbf{B}} \equiv \mathbf{B}/|\mathbf{B}|$. Expanding the field as $\mathbf{B}(z) \approx \mathbf{B}_0 + (\mathbf{B}'_\parallel + \mathbf{B}'_\perp)z + O(z^2)$, where $\mathbf{B}'_\parallel$ is parallel to $\mathbf{B}_0$ and $\mathbf{B}'_\perp$ is perpendicular. We note that a change in the magnitude of $\mathbf{B}$ has an accumulating effect on the spin precession, i.e. the change in $\mathbf{f}$ grows with t. In contrast, a change in the direction of $\mathbf{B}$ has a fixed effect: from the perspective of the measurement, a rotation of $\mathbf{B}$ is equivalent to a rotation of both the initial state and the measured

component F_z. For small gradients $\partial_z \mathbf{B} \ll \mathbf{B}/l_{\text{atoms}}$, where l_{atoms} is the length of the cloud, we can ignore $\mathbf{B}'_\perp$. This approximation, along with the fact that $A_B^{n+2} = -A_B^n$, allows us to write

$$R(z, t) \approx \mathbb{I} + A_{B_0} \sin \omega(z) t + A_{B_0}^2 [1 - \cos \omega(z) t], \tag{C.4}$$

where $\omega(z) = \gamma_F |\mathbf{B}_0 + z \mathbf{B}'_\parallel|$.

In our trap, we observe an atomic density $\rho(z)$ well approximated by a Lorentzian $\rho(z) = w/\pi(z^2 + w^2)$ where w is the FWHM extent of the ensemble. The collective spin $\mathbf{F} \equiv \sum_i f^i$ then evolves as

$$\mathbf{F}(t) = \int dz\, \rho(z) R(z, t) \mathbf{f}(0) \tag{C.5}$$

$$= [\mathbb{I} + A_{B_0}^2] \mathbf{F}(0) + e^{-w \gamma_F |\mathbf{B}'_\parallel| t} (A_{B_0} \sin \omega_0 t - A_{B_0}^2 \cos \omega_0 t) \mathbf{F}(0). \tag{C.6}$$

In the first term $\mathbb{I} + A_{B_0}^2$ describes a projector onto the direction of $\mathbf{B}_0$. This is the steady-state polarization. The second line describes a decaying oscillation about $\mathbf{B}_0$ of the perpendicular components with a coherence time $T = 1/(w \gamma_F |\mathbf{B}'_\parallel|)$.

References

[1] Hammerer K, Sørensen A S and Polzik E S 2010 Quantum interface between light and atomic ensembles *Rev. Mod. Phys.* **82** 1041–93

[2] Julsgaard B, Sherson J, Ignacio Cirac J, Fiurasek J and Polzik E S 2004 Experimental demonstration of quantum memory for light *Nature* **432** 482–6

[3] Matsko A B, Novikova I, Welch G R, Budker D, Kimball D F and Rochester S M 2002 Vacuum squeezing in atomic media via self-rotation *Phys. Rev.* A **66** 043815

[4] Mikhailov E E and Novikova I f 2008 Low-frequency vacuum squeezing via polarization self-rotation in Rb vapor *Opt. Lett.* **33** 1213–5

[5] Giovannetti V, Lloyd S and Maccone L Quantum metrology *Phys. Rev. Lett.* **96** 010401

[6] Louchet-Chauvet A, Appel J, Renema J J, Oblak D, Kjaergaard N and Polzik E S 2010 Entanglement-assisted atomic clock beyond the projection noise limit *New J. Phys.* **12** 065032

[7] Napolitano M, Koschorreck M, Dubost B, Behbood N, Sewell R J and Mitchell M W 2011 Interaction-based quantum metrology showing scaling beyond the Heisenberg limit *Nature* **471** 486–9

[8] Sewell R J, Koschorreck M, Napolitano M, Dubost B, Behbood N and Mitchell M W 2012 Magnetic sensitivity beyond the projection noise limit by spin squeezing *Phys. Rev. Lett.* **109** 253605

[9] Braunstein S L and van Loock P 2005 Quantum information with continuous variables *Rev. Mod. Phys.* **77** 513–77

[10] Dubost B, Koschorreck M, Napolitano M, Behbood N, Sewell R J and Mitchell M W 2012 Efficient quantification of non-Gaussian spin distributions *Phys. Rev. Lett.* **108** 183602

[11] Giedke G and Ignacio Cirac J 2002 Characterization of Gaussian operations and distillation of Gaussian states *Phys. Rev.* A **66** 032316

[12] Kurucz Z and Mølmer K 2010 Multilevel Holstein-Primakoff approximation and its application to atomic spin squeezing and ensemble quantum memories *Phys. Rev.* A **81** 032314

[13] Kraus B, Hammerer K, Giedke G and Ignacio Cirac J 2003 Entanglement generation and Hamiltonian simulation in continuous-variable systems *Phys. Rev.* A **67** 042314

[14] Madsen L B and Mølmer K 2004 Spin squeezing and precision probing with light and samples of atoms in the Gaussian description *Phys. Rev.* A **70** 052324

[15] Hammerer C, Mølmer K, Polzik E S and Cirac J I 2004 Light–matter quantum interface *Phys. Rev.* A **70** 044304

[16] Mølmer K and Lars Bojer Madsen 2004 Estimation of a classical parameter with Gaussian probes: magnetometry with collective atomic spins *Phys. Rev.* A **70** 052102

[17] Koschorreck M and Mitchell M W 2009 Unified description of inhomogeneities, dissipation and transport in quantum light–atom interfaces *J. Phys. B: Atom. Mol. Opt. Phys.* **42** 195502

[18] de Echaniz S R, Koschorreck M, Napolitano M, Kubasik M and Mitchell M W 2008 Hamiltonian design in atom–light interactions with rubidium ensembles: a quantum-information toolbox *Phys. Rev.* A **77** 032316

[19] Norris L M, Trail C M, Jessen P S and Deutsch I H 2012 Enhanced squeezing of a collective spin via control of its qudit subsystems *Phys. Rev. Lett.* **109** 173603

[20] Smith G A, Chaudhury S, Silberfarb A, Deutsch I H and Jessen P S 2004 Continuous weak measurement and nonlinear dynamics in a cold spin ensemble *Phys. Rev. Lett.* **93** 163602

[21] Pustelny S, Koczwara M, Cincio Ł and Gawlik W 2011 Tailoring quantum superpositions with linearly polarized amplitude-modulated light *Phys. Rev.* A **83** 043832

[22] Chaudhury S, Smith A, Anderson B E, Ghose S and Jessen P S 2009 Quantum signatures of chaos in a kicked top *Nature* **461** 768–71

[23] Budker D, Kimball D F, Rochester S M and Yashchuk V V 2000 Nonlinear magneto-optical rotation via alignment-to-orientation conversion *Phys. Rev. Lett.* **85** 2088–91

[24] Pustelny S, Wojciechowski A, Gring M, Kotyrba M, Zachorowski J and Gawlik W 2008 Magnetometry based on nonlinear magneto-optical rotation with amplitude-modulated light *J. Appl. Phys.* **103** 063108

[25] Koschorreck M, Napolitano M, Dubost B and Mitchell M W 2010 Quantum nondemolition measurement of large-spin ensembles by dynamical decoupling *Phys. Rev. Lett.* **105** 093602

[26] Sewell R J, Napolitano M, Behbood N, Colangelo G and Mitchell M W 2013 Certified quantum non-demolition measurement of a macroscopic material system *Nature Photon.* **7** 517–20

[27] Acosta V M *et al* 2008 Production and detection of atomic hexadecapole at earth's magnetic field *Opt. Express* **16** 11423–30

[28] Dowling J P, Agarwal G S and Schleich W P 1994 Wigner distribution of a general angular-momentum state: applications to a collection of two-level atoms *Phys. Rev.* A **49** 4101–9

[29] Geremia J M, Stockton J K and Mabuchi H 2006 Tensor polarizability and dispersive quantum measurement of multilevel atoms *Phys. Rev.* A **73** 042112

[30] de Echaniz S R, Mitchell M W, Kubasik M, Koschorreck M, Crepaz H, Eschner J and Polzik E S 2005 Conditions for spin squeezing in a cold ^{87}RB ensemble *J. Opt. B: Quantum Semiclass. Opt.* **7** s548

[31] Deutsch I H and Jessen P S 2010 Quantum control and measurement of atomic spins in polarization spectroscopy *Opt. Commun.* **283** 681–94

[32] Juliá-Díaz B, Zibold T, Oberthaler M K, Melé-Messeguer M, Martorell J and Polls A 2012 Dynamic generation of spin-squeezed states in bosonic josephson junctions *Phys. Rev.* A **86** 023615

[33] Vasilyev D V, Hammerer K, Korolev N and Sørensen A S 2012 Quantum noise for faraday light–matter interfaces *J. Phys. B: Atom. Mol. Opt. Phys.* **45** 124007

[34] Petersen V and Mølmer K 2006 Estimation of fluctuating magnetic fields by an atomic magnetometer *Phys. Rev.* A **74** 043802

[35] Demoen B, Vanheuverzwijn P and Verbeure A 1977 Completely positive maps on the C.C.R-algebra *Lett. Math. Phys.* **2** 161–6

[36] Behbood N, Martin Ciurana F, Colangelo G, Napolitano M, Mitchell M W and Sewell R J 2013 Real-time vector field tracking with a cold-atom magnetometer *Appl. Phys. Lett.* **102** 173504

[37] Puentes G, Colangelo G, Sewell R J and Mitchell M W 2012 Planar quantum squeezing via quantum non-demolition measurements in cold atomic ensembles arXiv:1211.4862 [quant-ph]

[38] Koschorreck M, Napolitano M, Dubost B and Mitchell M W 2010 Sub-projection-noise sensitivity in broadband atomic magnetometry *Phys. Rev. Lett.* **104** 093602

[39] Kubasik M, Koschorreck M, Napolitano M, de Echaniz S R, Crepaz H, Eschner J, Polzik E S and Mitchell M W 2009 Polarization-based light–atom quantum interface with an all-optical trap *Phys. Rev.* A **79** 043815

[40] Windpassinger P J, Kubasik M, Koschorreck M, Boisen A, Kjrgaard N, Polzik E S and Mller J H 2009 Ultra low-noise differential ac-coupled photodetector for sensitive pulse detection applications *Meas. Sci. Technol.* **20** 055301

[41] Koschorreck M 2010 Generation of spin squeezing in an ensemble of cold rubidium 87 *PhD Thesis* Universitat Politecnica de Catalunya

[42] Tóth G and Mitchell M W 2010 Generation of macroscopic singlet states in atomic ensembles *New J. Phys.* **12** 053007

[43] Urizar-Lanz I, Hyllus P, Egusquiza I L, Mitchell M W and Tóth G 2013 Macroscopic singlet states for gradient magnetometry *Phys. Rev.* A **88** 013626